Fall 2003

Patterning layer -by -layer self -assembled multilayer by lithography and its applications to thin film devices

Feng Hua

Follow this and additional works at: https://digitalcommons.latech.edu/dissertations

PATTERNING LAYER-BY-LAYER SELF-ASSEMBLED

MULTILAYER BY LITHOGRAPHY AND ITS APPLICATIONS

TO THIN FILM DEVICES

By

Feng Hua, Ph.D.

A Dissertation Presented in Partial Fulfillment of the
Requirement for the Degree of
Doctor of Philosophy in Engineering

COLLEGE OF ENGINEERING AND SCIENCE
LOUISIANA TECH UNIVERSITY

[Sep 2003]

UMI Number: 3126860

INFORMATION TO USERS

The quality of this reproduction is dependent upon the quality of the copy submitted. Broken or indistinct print, colored or poor quality illustrations and photographs, print bleed-through, substandard margins, and improper alignment can adversely affect reproduction.

In the unlikely event that the author did not send a complete manuscript and there are missing pages, these will be noted. Also, if unauthorized copyright material had to be removed, a note will indicate the deletion.

UMI®

UMI Microform 3126860

Copyright 2004 by ProQuest Information and Learning Company.

All rights reserved. This microform edition is protected against unauthorized copying under Title 17, United States Code.

ProQuest Information and Learning Company
300 North Zeeb Road
P.O. Box 1346
Ann Arbor, MI 48106-1346

APPROVAL FOR SCHOLARLY DISSEMINATION

The author grants to the Prescott Memorial Library of Louisiana Tech University the right to reproduce, by appropriate methods, upon request, any or all portions of this Dissertation. It is understood that "proper request" consists of the agreement, on the part of the requesting party, that said reproduction is for his personal use and that subsequent reproduction will not occur without written approval of the author of this Dissertation. Further, any portions of the Dissertation used in books, papers, and other works must be appropriately referenced to this Dissertation.

Finally, the author of this Dissertation reserves the right to publish freely, in the literature, at any time, any or all portions of this Dissertation.
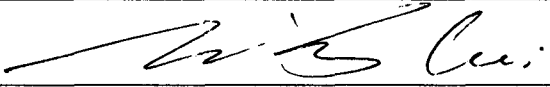
Author   Feng Hua

Date   Sep. 16. 03

GS Form 14
(5/03)

LOUISIANA TECH UNIVERSITY
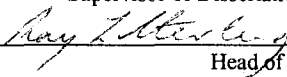
THE GRADUATE SCHOOL

9/15/2003

Date

We hereby recommend that the dissertation prepared under our supervision

by Feng Hua

entitled Patterning Layer-by-Layer Self-Assembled Thin Film by Lithography and

Its Applications to Thin Film Devices

be accepted in partial fulfillment of the requirements for the Degree of

Ph.D in Engineering

_____
Supervisor of Dissertation Research

_____
Head of Department

Ph.D in Engineering
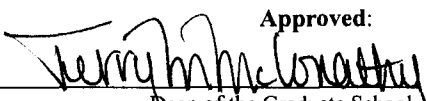Department

Recommendation concurred in:

Advisory Committee

Approved:

_____
Director of Graduate Studies

_____
Dean of the College

Approved:

_____
Dean of the Graduate School

ABSTRACT

Nanoparticles are exciting materials because they exhibit unique electronic, catalytic, and optical properties. As a novel and promising nanobuilding block, it attracts considerable research efforts in its integration into a wide variety of thin film devices.

Nanoparticles were adsorbed onto the substrate with layer-by-layer self-assembly which becomes of great interest due to its suitability in colloid particle assembly. Without extremely high temperatures and sophisticated equipment, molecularly organized films in an exactly pre-designed order can grow on almost all the substrates in nature.

Two approaches generating spatially separated patterns comprised of nanoparticles are demonstrated, as well as two approaches patterning more than one type of nanoparticle on a silicon wafer. The structure of the thin film patterned by these approaches are analyzed and considered suitable to the thin film device.

Finally, the combination of lithography and layer-by-layer (lbl) self-assembly is utilized to realize the microelectronic device with functional nanoparticles. The lbl self-assembly is the way to coat the nanoparticles and the lithography to pattern them. Based on the coating and patterning technique, a MOS-capacitor, a MOS field-effect-transistor and a magnetic thin film cantilever are fabricated.

TABLE OF CONTENTS

v

LIST OF TABLES

LIST OF FIGURES

viii

ACKNOWLEDGEMENTS

I wish to express my deep appreciation to my advisors, Dr. T. Cui and Dr. Y. Lvov, for their invaluable guidance, encouragement, patience, and generous support throughout my research and studies, and I also would like to express my special thanks to Dr. McShane, Dr Frank Ji, and Mr. Fang Ji for their generous advice and help during the completion of my dissertation. I am very grateful to those for graciously agreeing to take their precious time serving on my advisory committee and offering many valuable suggestions. Also, I would like to thank all the faculty and staff members as well as the graduate students of IFM for being supportive during various stages of this dissertation.

CHAPTER I

INTRODUCTION

1.1 Layer-by-Layer Self-Assembly

1.1.1 Principle

It is abundantly clear that the insatiable demand for new materials for emerging technologies is driving materials synthesis and change. Materials chemistry will play a central role in this endeavor through the creation of materials with structures and properties able to meet the demands required by up-and-coming technologies. Layer-by-layer (LbL) assembly is becoming a popular method for the synthesis of nanocomposite thin films and has attracted widespread interest in such nanohybrids.[1-7] The exciting feature of this approach is the ability to assemble complex structures rationally from designed modular components and integrate them into self-assembling constructions for a range of perceived applications. By creating a series of purposeful strategies, it is believed that truly revolutionary advances in materials science and technology can result from this approach. One layer-by-layer technique was developed in 1927 by Irving Langmuir, who won the Nobel Prize for other work, and Katherine Blodgett. The Langmuir-Blodgett assembly demonstrated that monolayers of fatty acids could be ordered on the surface of water by application of pressure undergoing phase changes from a gaseous state of

1

noninteracting molecules to a "solid" state where the molecules interacted in a rigid film. Langmuir and Blodgett implemented the transfer of such monolayers from the water surface to a solid substrate by slowly passing an appropriately treated substrate through the air/water interface. But, there have been no applications developed until now, although scientists found these techniques interesting for research. Other deposition techniques such as spin coating, physical/chemical vapor deposition, sputtering, etc. also find their applications in certain areas. Capable of coating bio and other nano materials, LbL self-assembly is being realized as one important method that is unique in many situations to construct ordered nano-scale thin films.

Layer-by-layer self-assembly can be regarded as an approach to bind basic building blocks in a designed structure and length scale. In a self-organizing system, basic construction-units spontaneously associate to form a particular structure, the architecture of which is solely determined by the bonding properties and shapes of the individual components. A stable structure is produced until a minimum system free energy state is reached. Self-assembly is usually entropically driven in an aqueous system, where association of modules is accompanied by exclusion of ordered water molecules. A feature of self-assembly is hierarchy, where primary building blocks associate into more complex secondary structures that are integrated into the next size level in the hierarchy. This organizational scheme continues until the highest level in the hierarchy is reached. These hierarchical constructions may exhibit unique properties that are not found in the individual components. Complexity and hierarchy is a characteristic of many self-assembling biological structures and is beginning to emerge as a hallmark of supramolecular materials. Part of the motivation for this emergence stems from the

notion that the architecture of complex macrosystems in biology and engineering physics are generally based on hierarchical building principles, i. e. smaller units are assembled into larger ones, which in turn are organized at a higher dimension. This construction process is continued until the highest level of structural complexity in the hierarchy has been attained.

The phenomenon of layer-by-layer adsorption of charged colloids was first demonstrated in 1966 by Iler. Electrostatic self-assembly was later extended to the multilayer of polyions, proteins and nanoparticles after the demonstration by Decher. It was found to provide robust, uniform, and long-lasting films.[8-12]

LbL self-assembly employs electrostatic interactions between anionic and cationic compounds (e. g. synthetic or natural polyions such as polyelectrolytes, DNA, proteins, or even colloids) which offer the following major advantages: [13-18]

- layer-by-layer construction due to surface charge reversal in each layer

- restriction to single layers due to repulsion between last layer and excess material

- precise control of step growth to even 1 nm

- low steric demand for interaction between oppositely charged ions

- deposition on almost any solvent-accessible surface

- low process temperature-- usually around room temperature

- simplicity& low cost-- principle and operation are simple without high requirement on equipment because only two beakers are necessary

- ability to preset structure

- bio-chemical compatible- capable of coating many bio-chemical materials; suitable for fabrication of catalytic devices or sensors

- ease of coating on the reverse side or inner side of the structure

- ease to be industrialized

The LbL self-assembled materials must be in either dispersion or solution which is dissociated to be positive or negatively charged in an aqueous environment. The alternate immersion of the surface allows the adsorption of compound monolayers onto the oppositely charged layers underneath. The interaction governing the spontaneous self-assembly includes mainly the electrostatic, covalent, and hydrogen bonding, and hydrophobic and other types of interactions.

The adsorptee appears charged in solution. For instance, an anion or cation will be dissociated from the backbone of a polyion so that it is locally positively or negatively charged. In the case of the nanoparticle in dispersion, the surface of the particle is treated to bring polarized molecular bodies to show electrical interaction.[19,20]

Once the substrate is immersed in the solution for a fixed time, the ions will be adsorbed onto the surface by electrostatic force. After a fixed time, the adsorption will reach saturation due to the shield from the electrical interaction. The terminate potential of the film is alternated continuously with the alternate immersion of different solutions. As a result, thin films can be adsorbed on layer by layer by immersing into oppositely charged solutions. The composite films can range from 1- 1000 nm with a definite knowledge of their composition and order.

The proof of the electrostatic interaction between adjacent layers is offered by an alternate change of water contact angle measured after deposition of each monolayer and

a linear buildup of film thickness with number of bilayers deposited shown by ellipsometry. See figure 1.1

(a)

(b)
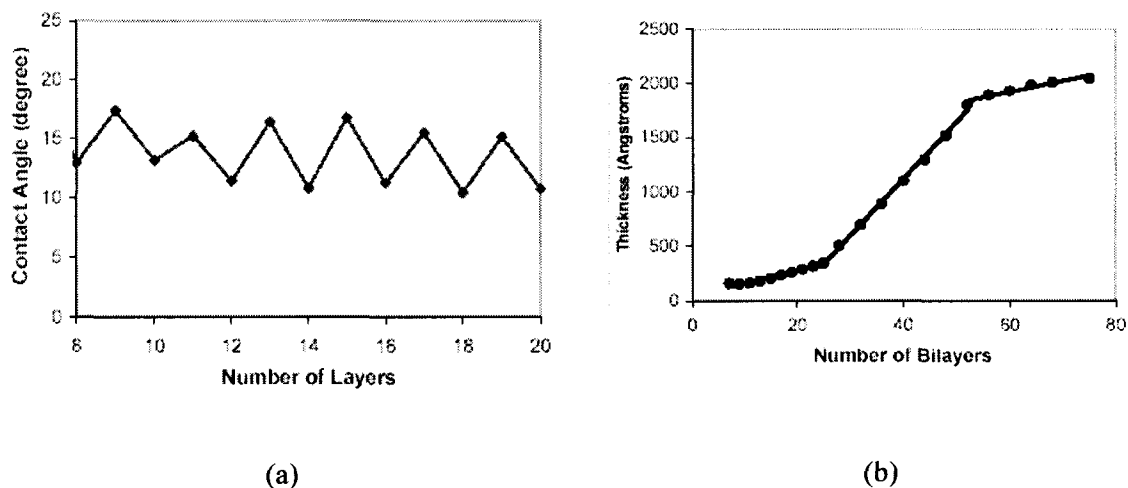
Fig. 1.1 (a) Water contact angle shift shows the change of surface characterization after each assembly. (b) Ellipsometry shows the even thickness growth of three

1.1.2 Building Blocks

There are hundreds of commercially available polyions that are employed to grow nanocomposite films. Polyions primarily used include (1) polycations- poly (ethylenimine) (PEI), poly (dimethyldiallylammonium chloride) (PDDA), poly(allylamine) (PAH), polylysine and chitosan; (2) polyanions- poly(styrenesulfonate) (PSS), poly(vinylsulfate), poly(acrylic acid), dextran sulfate, sodium alginate, heparin. (see fig. 1.2). Dyes primarily used include 3,'3'-disulfopropyl-5, 5'-dichloro-9-ethylthia-carbocyanine and azobenzene. Nanoparticles (metallic, semiconducting, magnetic, insulating) include gold, copper, ZnO, SnO_2, In_2O_3, TiO_2, Fe_2O_3, SiO_2 and clay

nanoplates. Proteins include cytochrome c, myoglobin, lysozyme, glucoamylase, and urease.

PSS   PDDA   PEI

Tailored nanoparticle
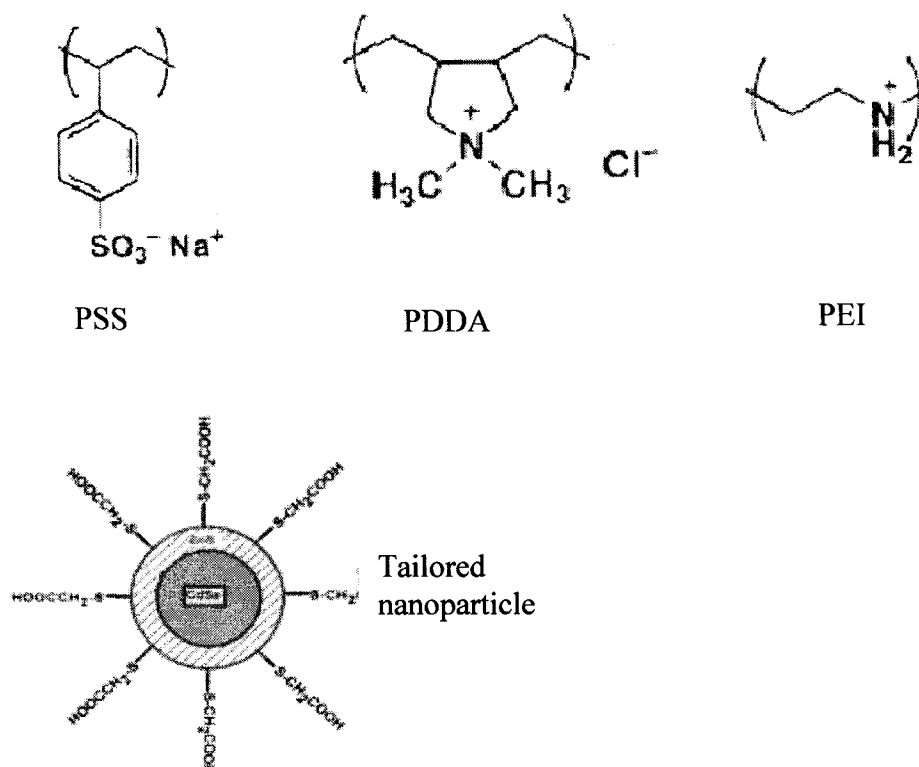
Fig. 1.2 Structure of LbL assembled materials

1.1.3 Procedure

LbL self-assembly has been developed into a well-established process to form quality and reproducible films. The standard procedure is as follows: (See fig. 1.3.)

1. Prepare aqueous solutions of polyion, nanoparticles or proteins at a concentration of 5-10 mg/ml. Adjust the pH value to ensure the components to be correctly charged.

2. Take a substrate carrying surface charge or treat it to be surface charged. Coat 5 layers of precursors to make the surface uniformly charged.

3. Alternately immerse the substrate into components' solutions for a fixed time with 1 min DI water rinsing.

4. Dry the sample by using a parallel nitrogen stream or spinning the sample.

5. Repeat the alternate immersion.

Before the preparation of desired layered structure, several layers of polyion precursors are usually helpful to the subsequent adsorption. This is the case especially when the solid support is not uniformly or strongly polarized. The polyions which serve as the "electrostatic glue" can fill in the pit on the surface and layers of them can further improve the surface characterization so that it is usually done to make a tough foundation for the assembly.
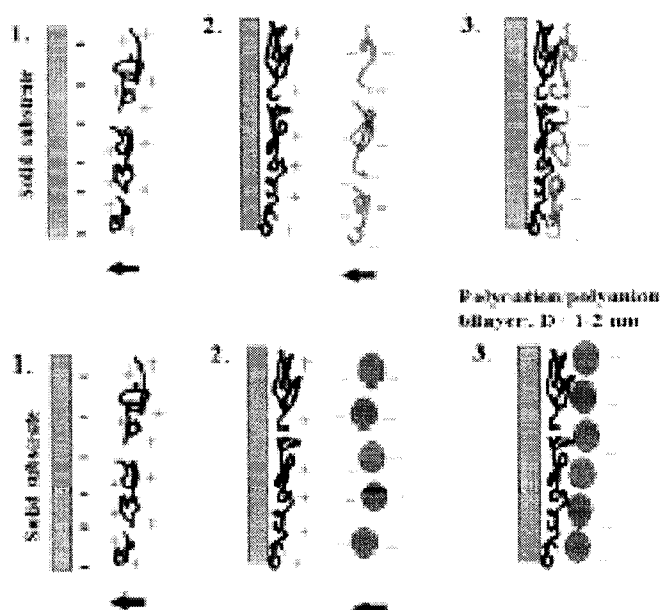
Fig. 1.3 Scheme of LbL self-assembly by alternate adsorption of polycations and negatively charged nanoparticles and polycations and polyanions.
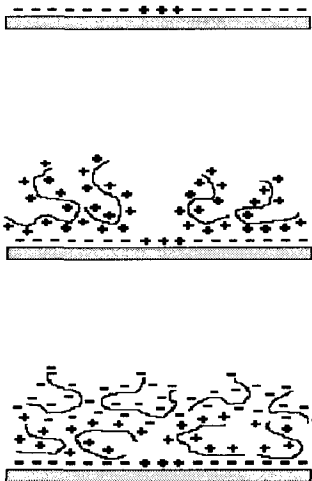
Fig. 1.4 precursor built-up to improve
the assembly.

1.1.4 Kinetics of LbL Self-Assembly

The quartz crystal microbalance (QCM) is an appropriate method in studying the

adsorption dependence of time. The QCM is a highly accurate quartz crystal

microbalance used for mass and viscosity measurements. It provides outputs related to

the series resonance frequency of the crystal oscillator to the mass changes of adsorbed or

deposited layers on a quartz crystal. The adsorption process can be monitored by QCM

for the purpose of establishing an optimized process, such as the saturation time,

concentration or PH. [21-23]

The relationship between the thickness of the adsorbed thin films and the shift of

the QCM resonance frequency follows the Sauerbrey equation which is written as:

Thickness= 0.02 x Δ (frequency) (nm)   (1)

The general procedure starts with preparing a QCM with a clean surface. Read its

original frequency on a digital frequency reader. Coat one layer of thin film. Wash it with

DI water and dry it with nitrogen stream. Read again the frequency which is different

from the original value. Compute the thickness growth of the thin film by the Sauerbrey equation. Coat the next layer and repeat this layer after layer. A plot of adsorption process versus the immersion cycle can be obtained. Process can be therefore optimized by monitoring this plot to achieve a large and stable growth step. Fig. 1.5a is a typical alternate adsorption plot of polyions (PDDA and PSS and silica).

In the same way, the QCM can be used to monitor only the time dependence of the adsorption to help understand the physical insight the process. Figure 1.5b shows the typical adsorption pattern of two consecutive assemblies of polycation (PAH) and polyanion (PSS) concentration of 1-3 mg/ml. The adsorption as a function of time can be regressed to an exponential curve which best fits the experimental data. It demonstrates that during the first 5 min around 87% of the material is adsorbed onto the charged surface and the next 3 min, e.g. at 8 min, brings down 95% of the material. Ten min is a normal immersion time to reach full saturation. In most publications, adsorption times of 5 to 20 min are commonly used. The process has its tolerance on time since once the saturation regime is reached, one or two minutes difference exerts no effect on the thickness of the film.

It shows that several minutes of DI water rinsing will remove those weakly attached materials from saturated surface.[24,25] The rinsing ensures that all materials adsorbed have been electrically or chemically bonded to the bottom layer. It also guarantees the precise step growth of LbL self-assembled thin films because only those attached with intrinsic interactions of LbL self-assembly are likely to anchor on the support while those precipitated on the support are removed by rinsing. In short, even though the adsorption time is different, as long as the saturation of adsorption is reached,

the water washing will provide the LbL assembled films with an identical growth thickness.
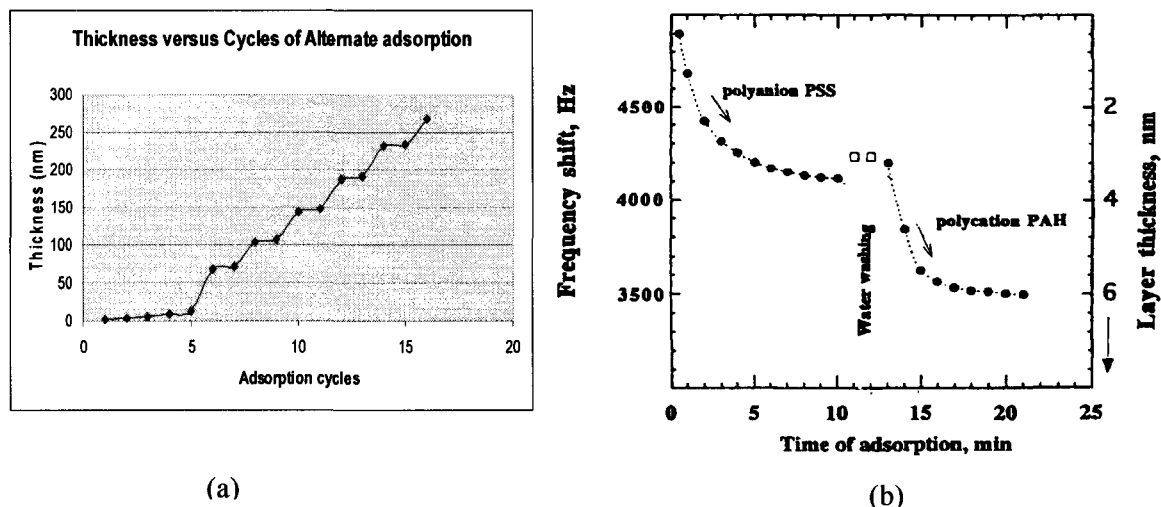
Fig. 1.5 (a) QCM measured adsorption curve of polyions and nanoparticle, concentration of 5 mg/ml, adsorption time PDDA and PSS 10 min, colloidal silica 2.5 min, 1 min intermediate water rinsing (b) QCM frequency shift in dependence of time, two steps of assembly of polycation (PAH) and polyanion (PSS), concentration of 3 mg/ml, PH 3.5, solution ionic strength 1 M NaCl.

1.1.5 Multilayer Structure

Self-assembled mono- and multilayer films on solid substrates have generated considerable interests recently because of the potential for controlling the molecular architecture and chemical and physical properties of layered assemblies on surfaces. The self-assembly technique provides an ordered thin film fabricated in the molecular level. The self-assembled monolayer (SAM) is stabilized by various interactions in the monolayer. The first part is the head group that provides the most exothermic process, i.e., chemisorption on the substrate surface. As a result of the exothermic head group-

substrate interactions, molecules try to occupy every available binding site on the surface, and in this process they push together molecules that have already adsorbed. The second part is the body, and the energies associated with its interchain van der Waals interations are on the order of a few. The third molecular part is the terminal functionality, which governs surface properties and makes it possible to form multilayer films. Molecular clusters and other molecules may be used to replace one or both of the polymer layers. Clusters, dipolar molecules, cage-structured and other molecules allow a wider design space for materials and devices.
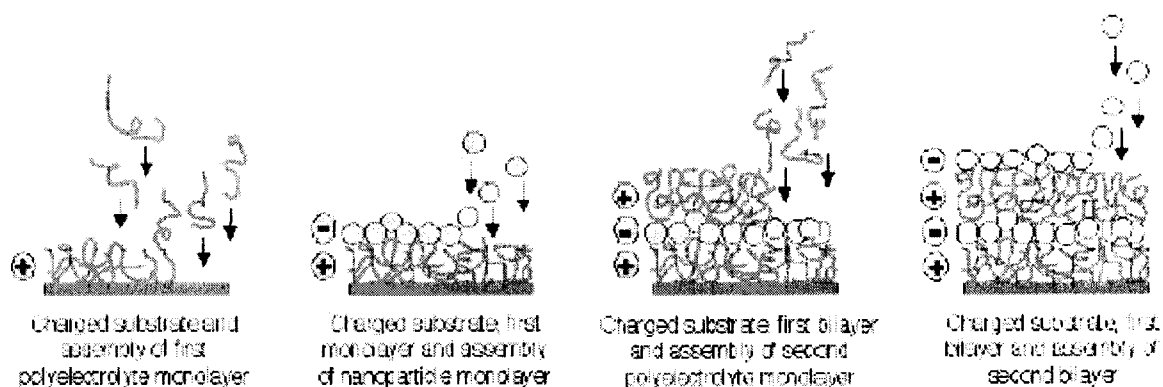
Fig. 1.6 Scheme of LbL self-assembled multilayer structure with different compositions.

"X-rays" or neutron reflectivity measurements of polyion films reveals the intrinsic well-ordered structure demonstrated by intensity oscillations, which are called Kiessig fringes due to the interference of radiation beams reflected from solid-support film and air-film interfaces.[26-30] The film thickness can be figured out from the periodicity of the oscillations with the Bragg-like equation. The values in fig. 1.7(a)

correspond to a growth step of polyion of about 1-2 nm in one cycle of excess adsorption and the nanoparticle-polyion bilayers thickness is determined by the diameter of the particle.
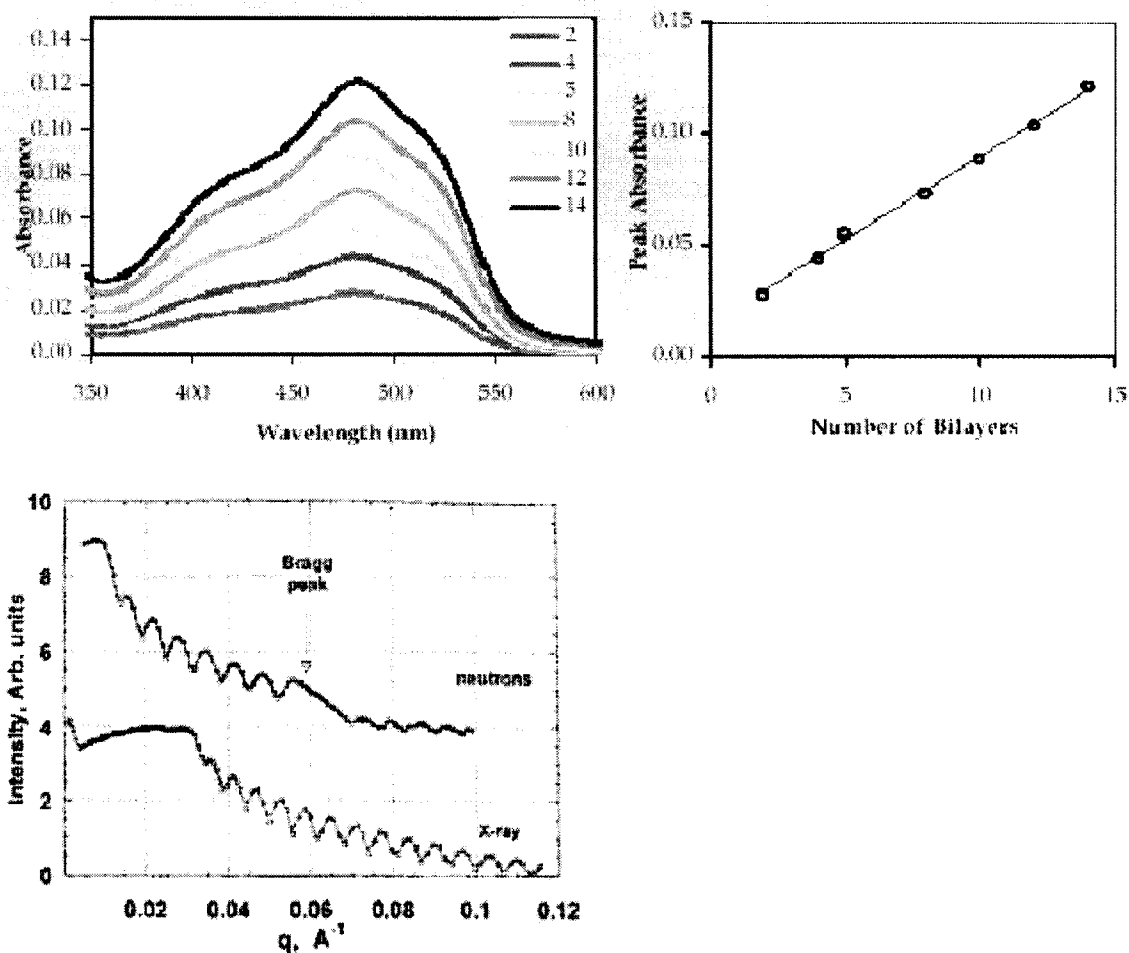
Fig. 1.7 (Top) UV absorption vs. the growth of the thin film. (Bottom) Intensity of X-ray and neutron reflection for PSS/myoglobin/PSS-d/myoglobin film

Neutron reflectivity analysis of films composed of deuterated PSS and hydrogen-containing PAH has proved that the polyanion-polycation films possess a highly uniform thickness as well as a well-ordered multilayer structure which can be predetermined. In

order to have a distinct spatial separation of components, the intermediate polyion layer needs to be thicker.

Another analysis of the layered structure comes from UV-vis absorbance spectroscopy. The linear buildup of a number of bilayers deposited is shown by UV-vis absorbance spectroscopy in fig. 1.7(b). The absorbance of the UV light increases linearly to the growth of the thin film which is observed as uniform in the plot.

1.1.6 <u>LbL Self-Assembled Thin Film</u>

Chemical synthesis of nanostructures and hybrid organic-inorganic materials represent the fastest growing topics of today's chemistry. Being at the interface of traditional disciplines, these areas of science present rich research grounds with potentially strong fundamental and technological impact. Ultrasmall semiconductor, magnetic and metal clusters have been in the center of scientific research for over a decade. For a relatively short period of time, a number of unique effects previously unseen for the parent bulk materials have been discovered for such species owing the large contribution of surface atoms into the properties of the nanoscale materials. On the other hand, successful utilization of the new qualities as well as further investigation of their fundamental properties is resting on the development of new techniques suitable for processing of nanoparticles into functional nanostructures and devices. Particularly interesting and technologically important is the production of ordered nanoparticle systems.

The layer-by-layer nature of the deposition enables stratification of the films by controlling the sequence in which the layers of different species are deposited. Order becomes one of the most influential parameters governing the functioning of the material.

For instance, graded semiconducting films displaying the step-by-step change of the energy of conduction and valence bands in the assemblies made of CdTe nanoparticle layers of different diameters can be easily prepared. The gradual transition of the absolute energy levels improves electron injection from electrode into the nanoparticle layer, which increases the light efficiency of nanoparticle light-emitting diodes.

Alternation of the layers from nanoparticles and alumosilicates allows for the preparation of self-sustained LBL-assembled films that exhibit a number of interesting properties.[31-34] For instance, the unique optical, magnetic, catalytic, and mechanical characteristics of nanomaterials to such films can be imparted. Nanoparticles open exciting perspectives for the development of new biomaterials. With hollow 20-30 nm titania particles (nanoshells), one succeeded in making new biocompatible electrode coatings with ion-selective properties, which are able to determine low concentrations of dopamine, one of the primary neurotransmitters, on the background of glucose. Self-standing membranes from nanoparticles can also be made with proteins and other biological macromolecules. In particular, an LbL overcoat from the latter may be used for improving nanoparticle biocompatibility of nanoparticles.

1.2 Patterning Layer-by-Layer Self-Assembled Nanoparticle

Nanoparticles have been the focus of many material researchers due to their unique properties in the microelectronics, optoelectronics and chemical fields.[35-38] A great deal of attention has been payed to the various potential applications of nanoparticles in complex nanoelectronic devices, photonic crystals, and biochemical sensors. Among numerous nanoparticle deposition techniques, LbL self-assembly has become an increasingly popular technique, which enables adsorption of colloidal

nanoparticles onto almost any material, due to its simplicity and versatility since its introduction by Decher et al. The alternate immersion of substrate in oppositely charged solutions allows thin films of nanoparticles, enzymes, or proteins in nanometer scale to be coated by electrostatic interaction.

There are works on application of the layer-by-layer assembly on two-dimensional (2-D) patterns.[39-48] These are based mostly on the microprinting of thiol compounds on gold and further assembly of the polyion multilayers on charged patterns, developed by Hammond et al. This strategy is designed to produce patterns by stamping onto substrates chemicals with different functionalities, i.e. polyion adhesive or resisting. The polyions were directed only to charge "attractive" regions and were repelled from the resistant regions. Whitesides et al crystallized latex particles in capillary channels produced by PDMS micromolding and made 3-D ensembles of 450-nm spheres with resolution of ca.1 μm. In another approach, poly(pyrrole) and poly(styrenesulfonate) were LbL-assembled on the 2-D charged micropattern produced on fluoropolymer by plasma treatment. The three methods described were quite successful, but restricted in applications by substrate materials (gold, fluoropolymers) or by necessity of special plastic stamps. Another challenge prior to device fabrication is to pattern two or more types of nanoparticles on one wafer. Hammond and T. Vossmeyer groups demonstrated their approaches to introduce two types of nanoparticles in the matrix by selective deposition technique.

Another approach to realize 2-D patterning of self-assembled multilayers is by silicon based lithographical technology,[49-51] which is a well established industrial process. By using this method, we avoid the selective deposition which demands strict

control and consequently obtain extremely high reproducibility and a simplified process. Since layer-by-layer self-assembly and lithography techniques are mature processes and lithography is widely applied to the modern semiconductor industry, a combinative technique will be economic and suitable for mass production. By just following the traditional process, the nanostructures comprised of nano-building bricks can be realized. As it behaves in the semiconductor industry, the process results in such a high reproducibility that distinct patterns (in this experiment 10 μm) can be created in almost all the dies on the wafer. Commercial electronic and photonic devices, such as MOSFET or solar cells with nanostructure are expected to be fabricated by this method at considerably lower cost and temperature. Layer-by-layer self-assembly was employed to deposit the nanoparticle-based thin film on a substrate while using a semiconductor process to pattern the thin film.

Both methods give patterns of approximately the same quality with minimal elements about 1-2 μm, edge roughness about 0.1-0.2 μm, and clear support surface between the pattern features. One of the advantages of our lithographic approach is that it is compatible with existing silicon micromanufacturing technology. This means that for an industrial application, existing silicon technology can be used to produce a 4" diameter silicon wafer completely covered with needed patterns of nanoparticle multilayers. With the microprinting approach, it is difficult to produce a perfect pattern on a surface area of more than a few mm^2. On the other hand, in the microprinting approach one can assemble biological (protein, DNA) multilayers on charged patterns. It is more difficult in the lithographic approach because of the need to dissolve in an organic solvent photoresist underlayer at the final stage of the process. In recent developments, polyion stamping on

supports other than gold and the possibility of filling gaps between polyion/nanoparticle strips with the second component through hydrogen bonding was elaborated. In the lithographic approach it is also possible to fill gaps between LbL assembled strips with a second component using metal mask etching and oxygen plasma treatment similar to the approach used in VLSI (Very Large Scale Integrated Circuits) industry.

1.2.1   Micro-Contact Printing

The micropatterning technique is demonstrated for ionic multilayer assembly, ranging from polyions to charged colloids. In this approach, polyions adsorb only to specific regions of a patterned functionalized surface; the surface acts as a molecular template for the sequential micro-patterned deposition of ionic polymer multilayers. This method allows the formation of patterned films using an inexpensive, simple one-step procedure performed on a laboratory bench top rather than a clean room. The ease and simplicity of the technique make it an accessible means of incorporating a number of passive and active organic multilayer systems into electro-optical devices. A significant discovery was that the pattern is reversed at high ionic strength, resulting in deposition on the regions which were originally resistant to adsorption, and no adsorption on the ionizable surface. From this work, it was discovered that by changing adsorption conditions, more complex composite films may be formed.

With the ability to fine-tune the adsorption conditions and the surface chemistry, we can optimize conditions for the formation of devices on gold, ITO glass or even plastic. Lateral or vertical composite films can be formed by directed deposition of two different polyion systems on different regions of a pattern. The following figure illustrates very recent results of a patterned film formed by adsorbing a strong polycation

with a sulfonated blue dye on the exterior (dark) regions, followed by a capping step, and

the subsequent adsorption of polyallylamine with a RuBpy dye. In this manner, more

than one color or electro-optical functionality can be placed in different regions of the

surface. The schematic of the microcontact printing is shown in figure 1.9.
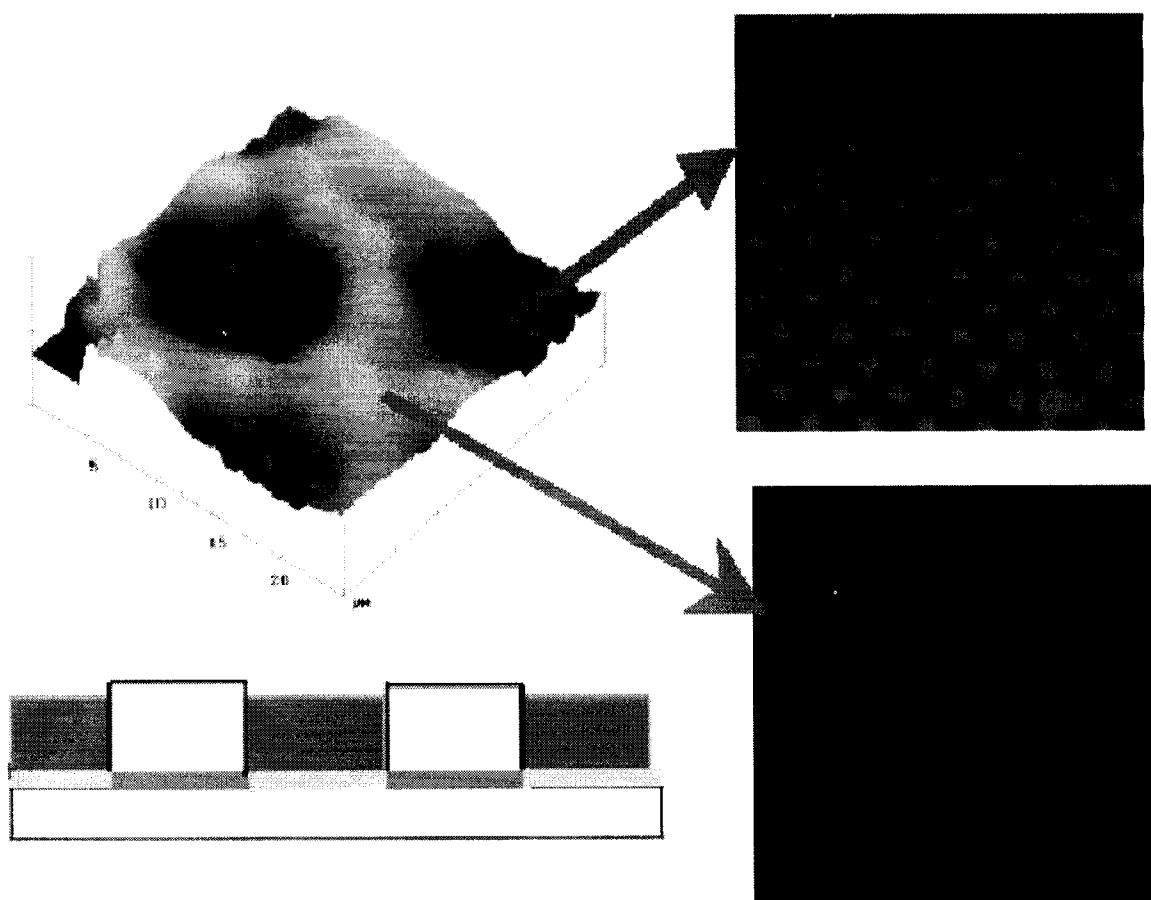
Figure 1.8. Atomic force micrograph showing two component, laterally patterned polyelectrolyte multilayers (left). By using hydrophobic or hydrophilic polyamines as co-polyions, blue and red electrochemiluminescent dyes can be directed to different regions of the surface (right).

Au/Cr →

Pattern transfer
by stamping

Thiol 16-mercaptohexadecanoic
acid (COOH), adhesion-
promoting

11-mercaptoundecanoic
triethyleneglycol (EG)
SAM, adhesion resisting

Polyelectrolyte multilayer
adsorption onto COOH
regions

Expose polyelectrolyte
surface to colloidal
slurry (SiO$_2$, PS)

Rinse off excess
slurry, dry
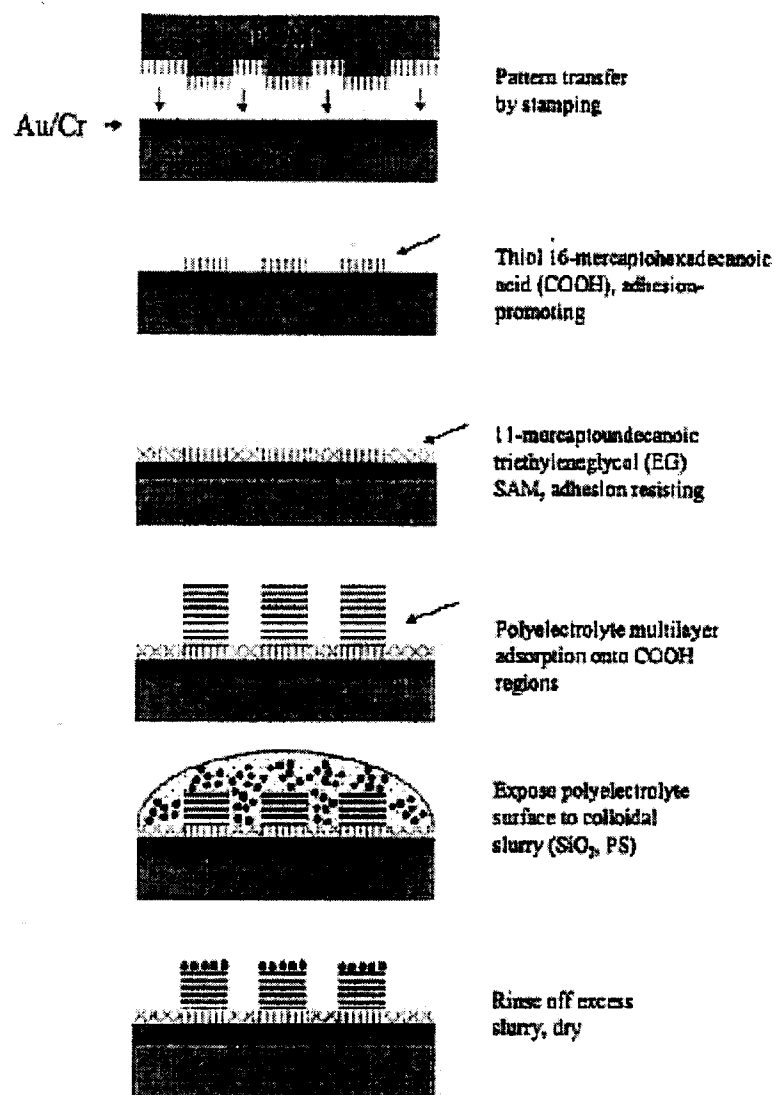
Figure 1.9. Schematic of microcontact printing: substrate patterning, polyelectrolyte adsorption, and colloid deposition.

1.2.2 Lithographic Patterning

We are the first research group to employ the well-established semiconductive process in the shape generation of layer-by-layer self-assembled thin film on the silicon wafer. The thin film is coated on the entire surface of the solid support instead of selective deposition on certain areas on the prepared template with more chemicals involved as microcontact printing does. Thus, we avoid the delicate directed assembly

which gives rise to a simple process. Of course, since the etching step is not eliminated in this method, the resolution and contamination is a factor that must be taken into account.

We have developed two methods in the spatial patterning of one type of nanoparticle thin film and two other methods for more than one type of nanoparticles which are coated on silicon wafer with layer-by-layer self-assembly. All of the process consists of ordinary lithographic steps. It appears that with the combination of various lithographic means, different approaches can be worked out in this application. The processes will be interpreted in detail in next chapter.

1.3 Concept of Combination of Lithography and LbL Self-Assembly

for the Fabrication of A Thin Film Device on Silicon Wafer

Based on the patterning approaches we developed, we created the concept of fabricating the thin film device by a combined technique of lithography and LbL self-assembly. This is a bottom to up technique which has already attracted more and more attention from researchers. We planned to incorporate functional nanoparticles into the thin film device. The nanoparticle thin film is produced by layer-by-layer molecular self-assembly and is patterned with traditional lithography. The first advantage of this process will be simple and cheap. Since only two beakers are needed, no extra coating instrument is necessary. The thin film deposition is carried out under room temperature; therefore, the temperature budget is not significant. The composition of the multilayer thin film can be predesigned by designing the sequence of deposition of different building blocks. The thickness of each monolayer is under precise control because the step growth can reach even as small as 1 nm. In short, it enables us to produce a device structures with definite knowledge of the composition and precise control of the thickness. It is extremely useful

to those complex devices such as organic LED or photovoltaic cell where the thickness of each organic thin film must be accurate. The layer-by-layer self-assembly consists of a series of regular dipping motions; its automation in production is predictable. Finally, since both of them are already mature, their combination will provide us with a reliable and flexible process in the thin film device fabrication. We have successfully produced several types of devices composed of different nanoparticles which will be discussed in the later chapters.

1.4   Current Self-Assembled Nanoparticle/Polyelectrolyte Device

Ultrathin films are currently attracting interest in many areas such as integrated optics and electronics. It is most interesting and challenging to construct films with a supermolecular architecture in which the individual organic molecules are macroscopically oriented and in which molecular with different functionality can be incorporated into individual layers. Unfortunately, traditional thin film processing techniques such as spin coating do not provide this level of control. It has been demonstrated that it is possible to build up multilayer thin films on a charged surface via the alternate deposition of polyanions and polycations. This method is an extremely simple layer-by-layer deposition process that can be used to fabricate complex devices based on multilayer heterostructures.[52-57]

Rectifying self-assembled ultrathin films have already been discovered. A Schottky diode can be readily made at the interface between multilayers of semiconducting nanoparticles (capped or uncapped) and a metallic conductor deposited onto it, as shown in figure 1.10.

Schottky behavior has been demonstrated in layer-by-layer assembled ITO/PPV/(HDT/CdSe)n/metal films, where PPV is the electroluminescent conducting
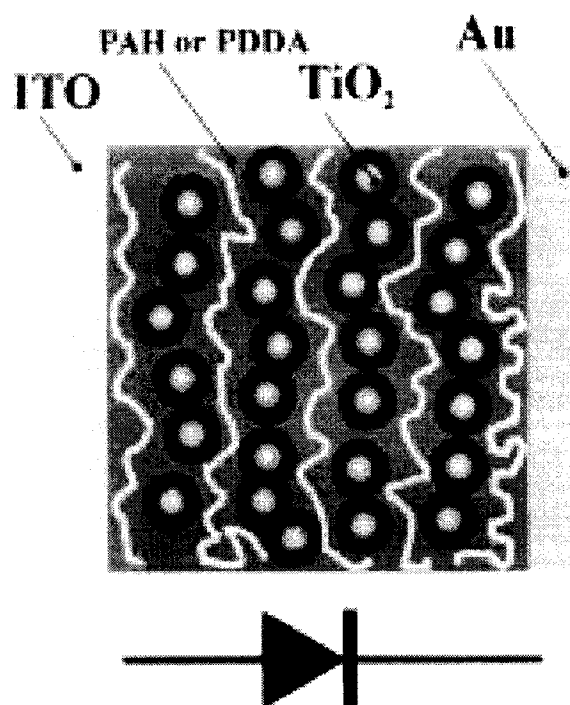
Figure 1.10. Schematic representation of a Schottky diode junction formed at the interface of TiO2/Au by the layer-by-layer self-assembly of n-type TiO2 nanoparticles (capped by 11-aminoundecanoic acid) and polyelectrolytes [poly (allylamine hydrochloride), PAH, or PDDA] onto an indium tin oxide (ITO)-coated glass electrode. Electrical contact was created by evaporating a thin layer of gold film on top of the ultrathin self-assembled film.

polymer poly(phenylene vinylene); the multilayers of PDDA/TiO2 nanoparticles (capped and uncapped), where PDDA is the polycationic polymer poly-(diallyldimethylammonium chloride); and films of ITO/(PDDA/TiO2 nanoparticles)

10/(PDDA/GO)$_{30}$/ PDDA/Au, where GO is graphite oxide. In the last case, the interface

of TiO$_2$/GO was found to be rectifying, suggesting that GO (oxidized to 25%) was still

graphitic enough to behave as a metallic-like material. Figure 1.11 shows the I-V

characteristics obtained by using TiO$_2$ nanoparticles 2.3 nm in diameter as an n-type

semiconductor. These junctions, made of 3–10 nanoparticle/binder bilayers, generally

exhibit a barrier height of 0.4–1 V when using ITO and Au as the cathode and anode,

respectively. Another type of composite layered rectifier has been recently developed

from a Ru(bpy)$^{32+}$ polymer, TiO$_2$ nanoparticles, GO, and polyelectrolytes as a binder.

Sequential deposition of these materials in an appropriate order resulted in double

rectifications (i.e., both at negative and at positive bias) due to the interface of TiO$_2$/GO

at a negative voltage and due to the electrochemistry of the redox polymer at a positive

voltage.
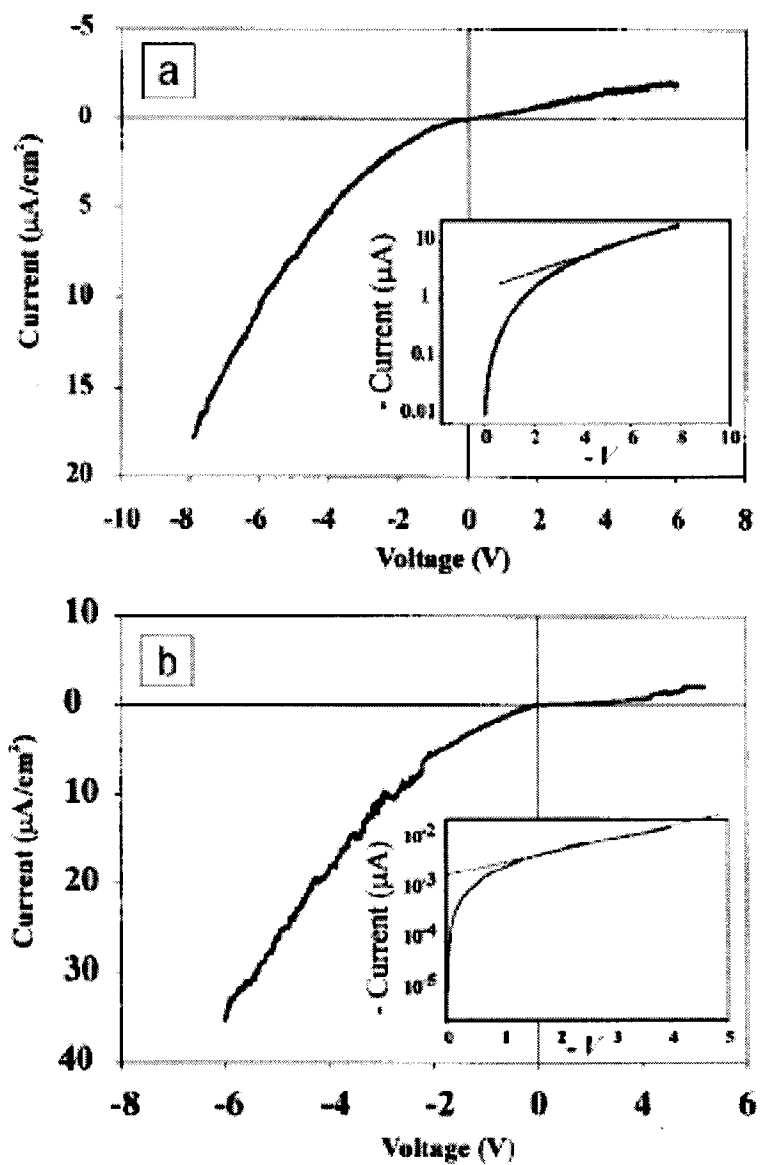
Figure 1.11. I-V characteristics of the systems (a) ITO/ $(PDDA/TiO_2)_{10}/Au$, and (b) ITO/ $(PDDA/TiO_2)_{10}/$ $(PDDA/GO)_{30}/Au$, where GO is graphite oxide. In both films, a Schottky diode is obtained, as evidenced by the insets showing the existence of a linear dependence of Log(I) versus V. The barrier heights were found to be 0.80 eV in (a) and 0.42 eV in (b).

CHAPTER II

PATTERNING LbL SELF-ASSEMBLED THIN FILM

2.1. Patterning One Type of Nanoparticle

Patterning one type of nanoparticle on silicon wafer with standard 4-inch wafer process is the starting point for creating complex shapes. In the following, two approaches are presented to generate nanoparticle patterns, showing the versatility and flexibility of the process.

2.1.1. Modified Lift-Off

Materials involved are the following: sodium poly(styrenesulfonate) (PSS) 3 mg/mL, MW 70K, 0.5 M NaCl; poly(dimethyldiallyl ammonium chloride) (PDDA) 3 mg/mL, 0.5 M NaCl, pH 7 (all from Sigma-Aldrich); and dispersion of 300-nm diameter silica nanoparticles in 0.02 M NaCl, 1 mg/mL, pH 9 (Bang Inc),or 45-nm diameter fluoresbrite microspheres 2.5 mg/mL, 0.02 M NaCl (Polyscience Inc).

Silicon wafers (Silicon Inc.)were used. A spin-coating machine (Brewer Science), UV-lamp, and Az1813 photoresist were used for the lithography process. For analysis of the pattern structures, we used Scanning Electron Microscope(SEM, AMRAY), Olympus Epifluorescense Microscope, and Wyko RST white light interferometric microscope.

A silicon wafer was hydrophylizied by treatment with H_2SO_4 and H_2O_2 solution (volumes ratio 7:3) at 50 °C for 1 hour. Then, it was "hardbaked" at 115 °C on a hotplate

25

for 2~3 minutes to remove the moisture for the subsequent lithography. A 1 μm thick

photoresist layer was spun cast on the silicon wafer. It was irradiated by UV-lamp for 1.5

min, and the desired pattern on photomask was transferred to the surface of photoresist

by developing. The image consists of alternate 5 μm-wide strips and spaces. Then the

substrate was dipped into PDDA and PSS solutions alternatively, in the sequence of

[PDDA (10 minutes) + PSS (10 minutes)]$_2$+PDDA(10 minutes). The outermost layer was

positively charged, and then silica nanoparticles which were surface modified to be

negatively charged were adsorbed in the sequence of [PDDA (10 minutes) / silica (2.5

minutes)] $_3$. For each step, the substrate was rinsed by DI-water for 1 minute and dried by

nitrogen flow between immersions. Finally, the substrate was put into acetone solution

with ultrasonic treatment for 5 seconds to remove the photoresist. The schematic is

shown in figure 2.1.
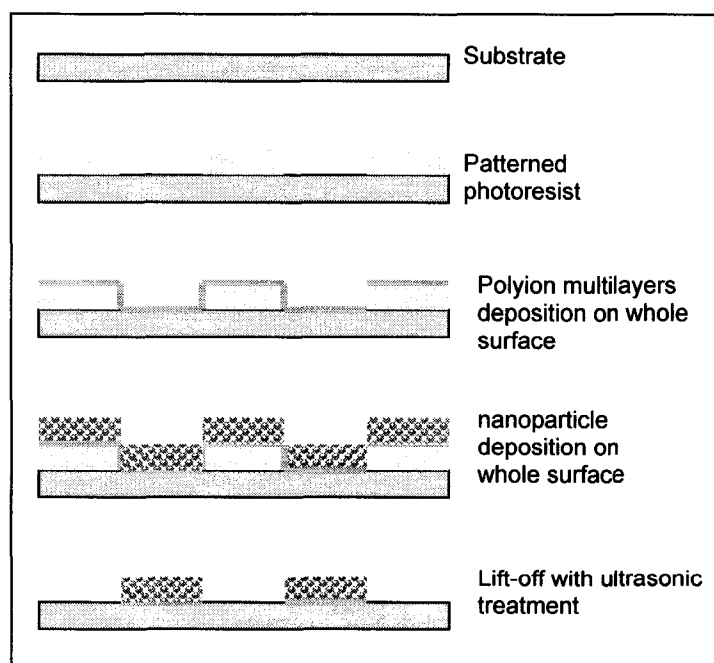
Fig. 2.1 Schematic of modified lift-off to pattern layer-by-layer
self-assembled nanoparticle thin film.

Clear and distinct images of nanoparticle strips on the resulted wafer were observed by SEM (Fig. 2.2a-c). The 5-μm strips containing the polyion precursor with nanoparticle multilayer are well shaped and have sharp borders. Silica nanoparticles are closely packed with few vacancy-defects. An average roughness of the strip borders is less than one particle diameter (in this case 200 nm, but it could be less if smaller particles are used). There are no particles in the areas between the strips. The cross section of the image is very spectacular: strips are evenly separated and shaped and have the same height 3000 nm. The height of the strip may be controlled with LbL assembly. In the present experiment we performed three steps of silica/PDDA deposition, and every step gave a 200-nm thickness increase what corresponds to a triple silica layer. One layer of thickness can be adjusted by lowing ion strength of silica dispersion.

These results indicate that polyion layers have pores big enough to let acetone molecules penetrate inside to dissolve photoresist and strip off the multilayers from these regions. The strip border sharpness indicates that intercalation length between neighboring molecules in polyion layer is less than 200 nm. In the control sample (Fig. 2.2d), during which the sample has not been sonicated during photoresist removing with acetone, the silicon wafer remains entirely covered by SiO_2 particles. The polyion layers as well as particles above them were not removed with photoresist and come back to the surface, which prevents the pattern formation. The collapse of the polyion layers and particles is due to the linkage among polyion molecules which is not disconnected at the edge of the photoresist sidewall by the process. Presence of particle clusters, instead of the pattern, visible at the Fig. 2.2d is due to incomplete removal of the polyion film located above the photoresist.
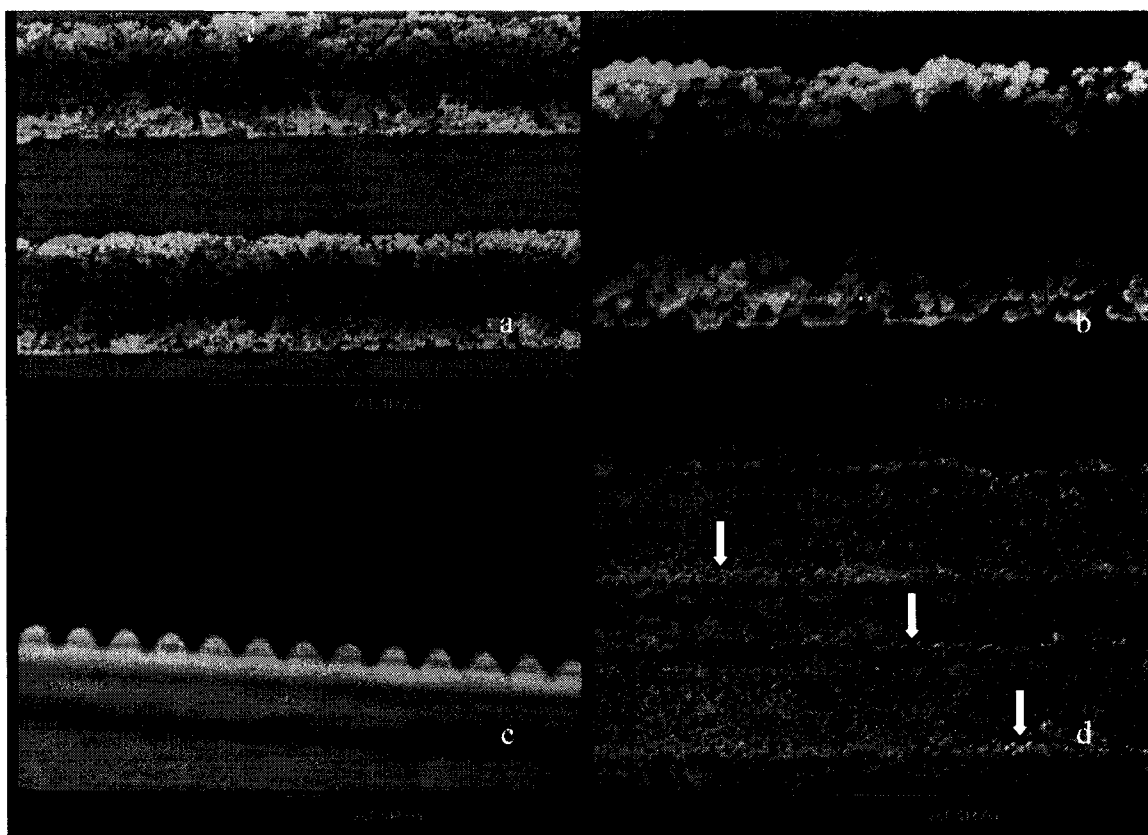
Fig. 2.2 SEM pictures of self-assembly patterns, (a-b) top view, (c) cross-section view; all with SiO₂ particles of 300 nm in diameter at the outermost layers. The line width is 5 μm. (d) SEM picture of control sample (lift-off technology without sonication). The arrows indicate those particles which were attached on sidewall.

This clean process also applies to the fluorescent materials. In another experiment, negatively charged 45-nm diameter fluorescent nanoparticles were assembled above similar precursor: {PEI + (PSS/PDDA)₃ + Fluoresbright/PDDA)₃} following the same experimental procedure. We used another mask with wider strips to provide a pattern well visible in fluorescent microscope (Fig. 2.3). One can see a sharp green pattern indicating a permanent coverage with width of the strips of 25-μm, and 12-μm wide dark areas without a fluorescent multilayer.
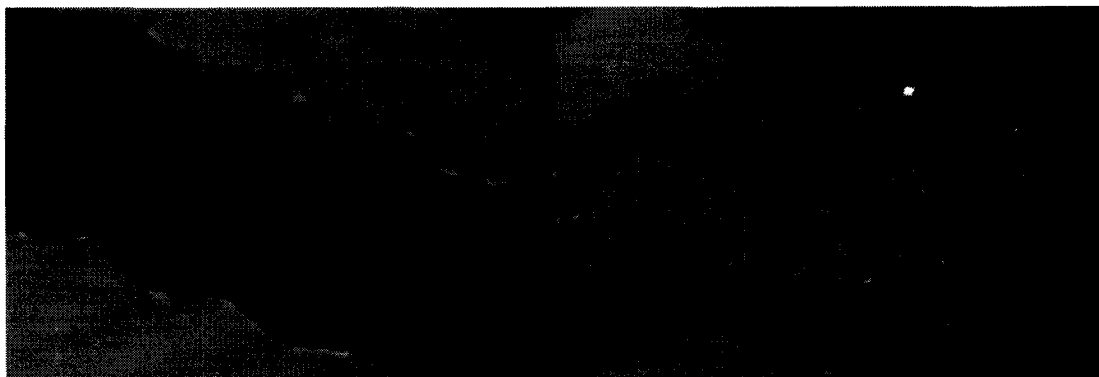
Fig. 2.3 Images of patterns of 25 μm width with fluorescent multilayer of {PEI + (PSS/PDDA)₃ + (Fluoresbright/PDDA)₃} composition produced on silicon with LbL-method (Olympus Epifluorescense Microscopy with a 530-filter and an exposure time 8 seconds).

2.1.2. Metal-Mask Method

Beside the modified lift-off, we also developed metal-mask method. Polyelectrolytes involved are poly(dimethyldiallyl ammonium chloride) (PDDA) aqueous solution, MW 200 to 300K, 3 mg/mL, 0.5 M NaCl and sodium poly(styrenesulfonate) (PSS) aqueous solution, MW 70K, 3 mg/mL, 0.5 M NaCl. They were obtained from Aldrich-Sigma. Dispersion of blue-dyed carboxylate modified polystyrene particle 300 nm in diameter was obtained from Seradyn Inc. The photoresist is Shipley AZ1813. Electronic-Vision dual side mask aligner EV420 from Electronic Visions, Inc. was used as the UV light illuminator. Aluminum layers were deposited by a DV-502A high-vacuum evaporator from Denton Vacuum, Inc. The 800 series micro RIE system from Technics Inc. was the etching facility to remove organic nanoparticles.

The schematic of the process is shown is in figure 2.4. The 4-inch silicon wafer was first put into sulfuric acid and hydrogen peroxide solution (volume ratio 3:7) at 70°C for 1 hour. It was immersed in 50 ml PDDA solution for 20 minutes. After that, it was rinsed in DI water for 1 minute and dried by nitrogen flow. It was then immersed in 50 ml PSS solution for 10 minutes, rinsed and dried as in the previous step. The cycle was repeated in a sequence of {PDDA (20 minutes) + [PSS (10 minutes) + PDDA (10 minutes)] $_2$}. The intermediate rinsing and drying are necessary. Finally, the outermost layer was positively charged PDDA. Then, it was immersed in 50 ml diluted polystyrene aqueous solution for 10 minutes (aqueous solution was made in a dispersion to water volume ratio of 1:9), rinsed and dried, these followed by another cycle of PDDA (10 minutes) + polystyrene (10 minutes). Therefore, the complete sequence of adsorption is {PDDA (20 minutes) + [PSS (10 minutes) + PDDA (10 minutes)]$_2$} + polystyrene (10 minutes) + PDDA (10 minutes) + polystyrene (10 minutes). To this point, a polystyrene nanoparticle thin film was produced on the wafer. It should be heated at 100° C for 10 minutes to get rid of the moisture in the films, and then aluminum was deposited by thermal evaporation. The deposition of aluminum was carried out at a pressure of 10^{-5} mTorr with a deposition rate of 2 angstroms per second until a thickness of 2500 angstroms was reached. After it was taken out of the vacuum chamber, a photoresist (AZ 1813) layer of one micron thick was spun on the aluminum at the maximum speed of 2000 rpm for 40 seconds. The photoresist was baked at 115° C on a hotplate for 1 minute. Then the silicon wafer was put on mask aligner, which is a UV light irradiation instrument with a chrome mask between the light source and the wafer. The time of exposure was set at 6 seconds. Later, it was developed by MF-319 developer for 30

seconds and rinsed by DI water. The aluminum etchant, phosphoric acid and nitric acid

(136g H_3PO_4 +5.5g H_3NO_3 per 100ml), was used to remove aluminum at 70°C for 2

minutes. It was put in the vacuum chamber of the reactive ion etching system. The

etching conditions were oxygen flow rate of 8 sccm, pressure of 110 mTorr, and electric

power of 250 w. The etching time is 5 minutes. The remained photoresist was removed

by acetone. The aluminum can be either removed by its etching solution or just left as an

electrode.
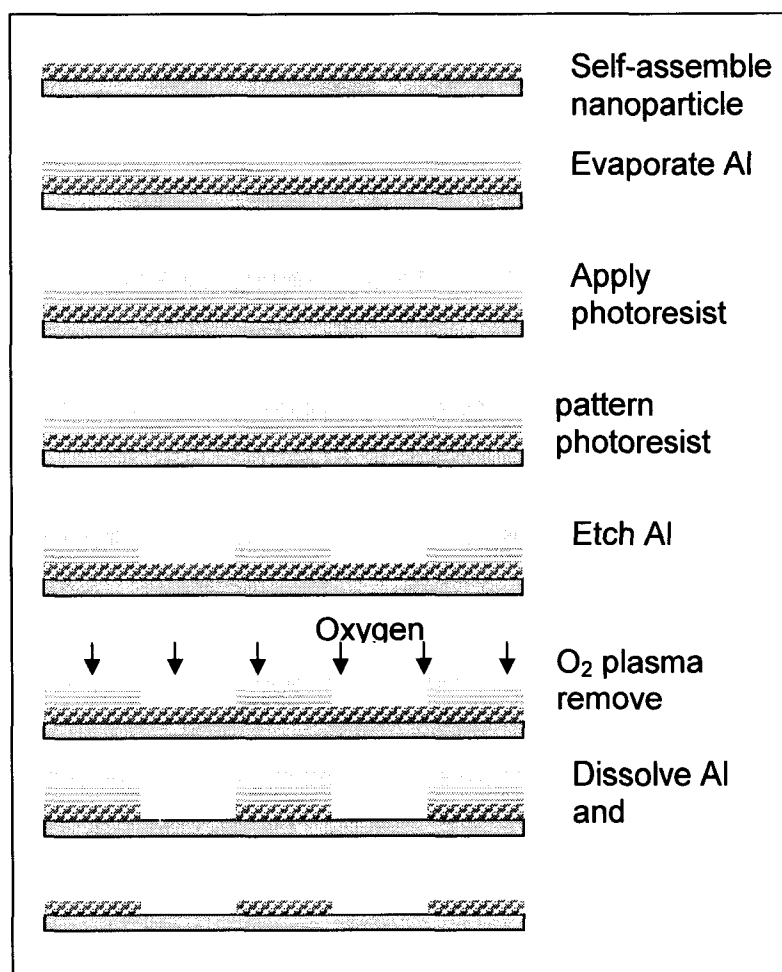
Fig. 2.4 Schematic of metal-mask method to pattern nanoparticle thin film

Two samples of polystyrene nanoparticles were prepared by this process. One was fixed on the stage of SEM for observation. Prior to taking picture, TiPt alloy was sputtered on the sample surface for 40 seconds at a pressure of 0.1 Torr and a current of 12mA. The scanning electron microscope was set up at 25 kV and maximum magnification of 20K. The SEM pictures were illustrated in Fig. 2.5.
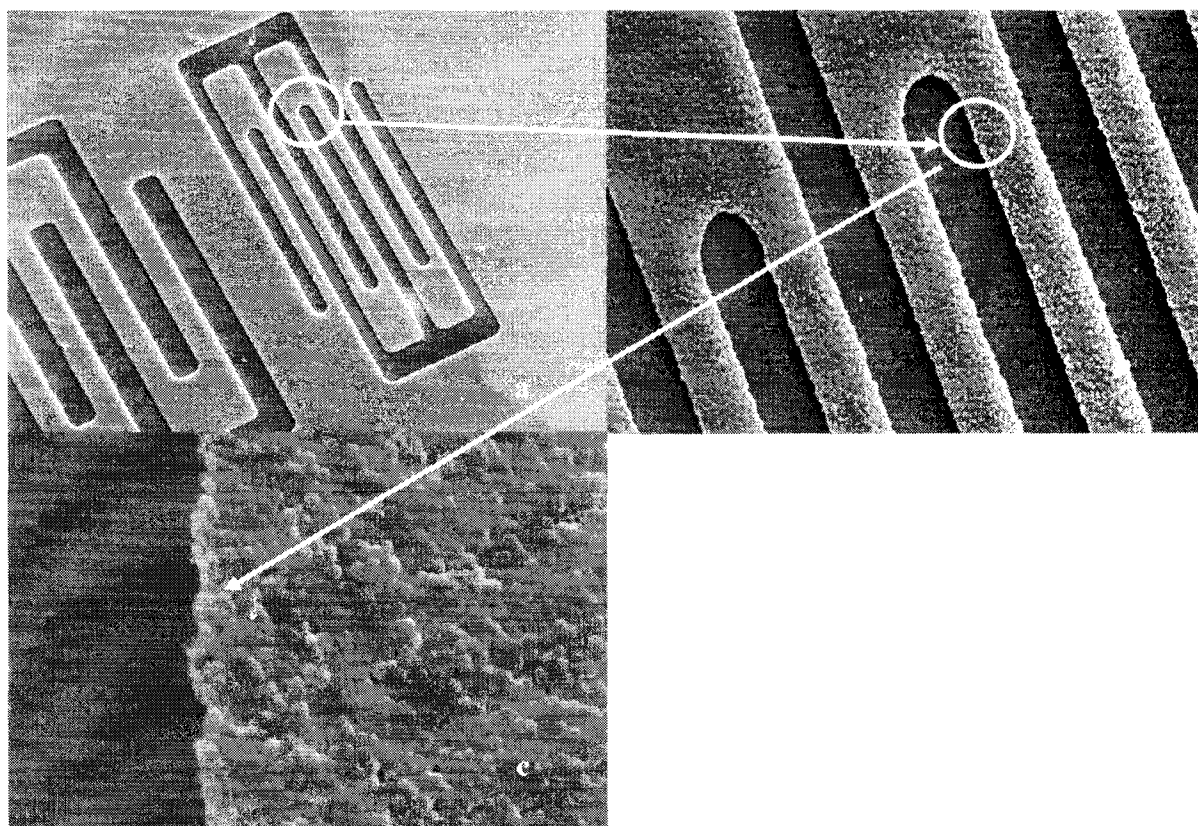
Fig. 2.5 SEM pictures of particle thin film. a). Full-size pattern of 300nm polystyrene particle thin film, line width is 10μm. b). Amplified circle area in (a). c). amplified circle area in (b).

The image on the mask has been faithfully embossed onto the nanoparticle thin film by the metal mask approach. Illustrated in Fig. 2.5, a comb-shaped pattern was generated with the particle occupied area, and the blank area separated clearly and sharply. Fig. 2.5 (a), (b), and (c) are pictures of one image at different magnifications. In

Fig. 2.5 (c), a sharp border along the blank area and particle covered area can be seen. It is quite interesting that many of the spherical particles along the border are observed to be cut in half. This is due to the bombardment of kinetic oxygen plasma, etching the particles that are not covered by the metal mask. This mechanism contributes to the straightness of the strip. Meanwhile, in the picture with the highest magnification, a rough edge about one particle diameter in size along the border can be observed. Obviously, this is because the border of metal mask is not perfectly sharp which may result from the roughness of the particle surface. The aluminum patterning is not carried out on the smooth silicon surface as in the usual case. On the contrary, it is deposited on the rough surface of the polystyrene particles. This may affect the uniformity of aluminum deposition and photoresist coating. The straightness of the border that results from a series of the process of deposition, UV exposure, and development is not as satisfactory as that on the smooth substrate. The approach was applied to both organic and inorganic particles so that it can be shown to be compatible to most of the important nanoparticles.

The principle of this approach is to use a metal layer as a mask when etching the nanoparticle layers underneath. The selection of metal is flexible. In our experiments, aluminum and chrome were chosen. Certainly, another optional material for the mask over nanoparticles is photoresist, and it may simplify the process greatly. The reason for avoiding resist in this experiment is that it is not suitable for the ultimate target of 3 dimensional nano-scale architecture fabrications. The first layer of resist remained as mask would be irradiated by the UV light when the second layer of photoresist is exposed. They will be dissolved with the second layer of photoresist together when undergoing the

second developing. As a result, the metal mask layer is the best way to avoid the issue addressed above.

2.1.3. Comparison of Two Methods

Both methods work well for the thin film patterning. As for the lift-off method (thereafter #1), it can be applied to all types of nanoparticles. In our second experiment, the metal mask method (thereafter #2) succeeds in controlling the spatial position of organic polystyrene particle by oxygen plasma etching. As a matter of fact, it can also be applied to inorganic particles if the appropriate recipe is available. If not, the flexibility of the mature semiconductor process can provide a simple wet etching to deal with it as a substitute to the dry etching.

Both methods can be applied to 3D fabrication as well as functional devices. In the 3D case, some factors have to be seriously controlled such as height, surface or border roughness and sidewall profile. The two methods can work out a 3D structure individually or both of them can be used if necessary. Table 2.1 shows the comparison of the two methods.

The border of #1 case is straighter than #2 case. The explanation stands on the fact that in #1 case, patterns on photoresist were made on the smooth silicon surface while in #2 case, patterns were made on a rough surface above the nanoparticle layer. This resulted in lines with different sharpness and eventually transferred onto the final patterns. It is quite interesting that almost all the polystyrene particles along the border had been cut in half, as shown in Fig. 2.5, because the ions in oxygen plasma with kinetic energy went straight down to the nanoparticle thin film. This played a role in improving the smoothness of the border, but this was not dominant.

However, the surface roughness of #2 is better than #1. The roughness step tester measured included average and rms roughness in surface roughness. The roughness of #1 is about 18% higher than #2. The difference in roughness can also be seen from the greater number of defects detected in #1 surface. This is due to the ultrasonic vibration in the process which is indispensable to break the polyion link and remove the nanoparticles above the resist. The defect in #1's structure is also attributed to another reason. If the nanoparticle layer is lower than the resist sidewall, some particles that used to attach on the wall were likely to come down along the wall during the resist dissolving step. Therefore, the height at two sides in #1 case is larger than that in the middle.

Because the #2 experienced etching process, it is more or less contaminated. Moreover, the blank area created by #2 is also dirtier than #1 since tiny residues were observed in SEM picture. This is resulted from the organic residue generated when the organic particles were etched by oxygen plasma.

Without a doubt, the most obvious advantage of #1 is its simplicity because fewer process procedures were involved.

	Metal mask	lift-off
Border sharpness		better
Surface roughness	better	
Defect in structure		more
Adhesion to substrate		better
contamination	more	
Channel cleanness		better
process		simple

Table 2.1. comparison of lift-off and metal mask methods

2.2. Patterning Multiple Types of Nanoparticles

The next challenge is to pattern more than one type of nanoparticle on a silicon wafer because even the simplest device may contain at least two substances. The vertical arrangement of nanoparticles is simple because the LbL self-assembly allows different types of nanoparticles to grow in an almost unlimited number of layers. We mainly demonstrate the ability to settle nanoparticles laterally on the surface.

2.2.1. Plasma Method

Materials involved are the same as above except the nanoparticles such as the blue-dyed carboxylate modified polystyrene particles, 150 nm in diameter, were obtained from Seradyn Inc. The polystyrene aqueous solution was made in dispersion to water volume ratio of 1:9. The silica nanoparticles dispersion (8 mg/mL) was diluted from Snow-Tex colloidal silica (40.9% wt%, PH 9.6, 78 nm in diameter) which was made by Nissan Chemical Industries, Ltd.

Initially, the 4-inch silicon wafer was put into sulfuric acid and hydrogen peroxide solution (volume ratio 3:7) at 70°C for 1 hour. 150 nm polystyrene particle thin film was then coated on the entire surface of silicon wafer by LbL self-assembly. The coating was done by alternate dipping in a sequence of: [PDDA (10 min) + PSS (10 min)]$_2$ + PDDA (10 min) + polystyrene (10 min). Intermediate rinsing and drying after each immersion are necessary. The rinsing was done by purging the wafer in the DI water flow for 1 min. The wafer was placed on a spinner and spun to remove water by centrifugal force. The maximum rotating speed was set at 1300 rpm for a time of 45 s. This drying method allows an even growth of nanoparticle thin film on the entire surface. It should be heated at 100° C for 3 minutes to completely remove moisture in the films, after which

aluminum was deposited by thermal evaporation. The deposition of aluminum was carried out at a pressure of 10^{-5} mtorr with a deposition rate of 2 Å/S until a thickness of 2500 Å was reached. After it was taken out of the vacuum chamber, a photoresist (AZ 1813) layer of one micron thick was spun on the aluminum at the maximum speed of 2000 rpm for 40 s. The photoresist was baked at $115^0 C$ on a hotplate for 1 min. Then the silicon wafer was placed on mask aligner to be exposed under UV light irradiation in order to transfer the pattern on the chrome mask to the photoresist. The time of exposure was set at 6 s. Later, it was developed by an MF-319 developer for 30 s and rinsed by DI water. The wafer should be placed under UV light for another 6 s to expose all the remaining photoresist. The aluminum etchant, phosphoric acid and nitric acid (136 g H_3PO_4 +5.5 g H_3NO_3 per 100 mL), were used at 70°C for 2 min to remove aluminum. The wafer was then put in the vacuum chamber of the reactive ion etching system to etch the polystyrene particle film. The etching conditions were the followings: an oxygen flow rate of 8 sccm, a pressure of 110 mTorr, and an electric power of 250 w. The etching time was 5 min. So far, the thin film of polystyrene nanoparticles had been patterned and remained covered by the aluminum and photoresist. Scraps sticking to the silicon surface remained which resulted from the oxygen bombardment upon the nanoparticle layer. The wafer was immersed in ultrasonic cleaner for 1 min to clean all of these scraps.

The 150 nm nanoparticles are now located in alternate with blank channel on silicon wafer. Next, 78 nm silica nanoparticles are filled into the channel using LbL self-assembly. The sequence of immersion was: [PDDA (10 min) + PSS (10 min)]$_2$ + PDDA (10 min) + silica (10 min). The intermediate rinsing and drying were still necessary and

were carried out as described above. The wafer was soaked into developer solution MF-319 for 10 min to dissolve photoresist and aluminum and during the first minute, the ultrasonic bath was introduced for roughly 3 s to improve the lift-off. Eventually, the pattern was obtained with two types of particles located next to each other. The schematic is shown in figure 2.6.
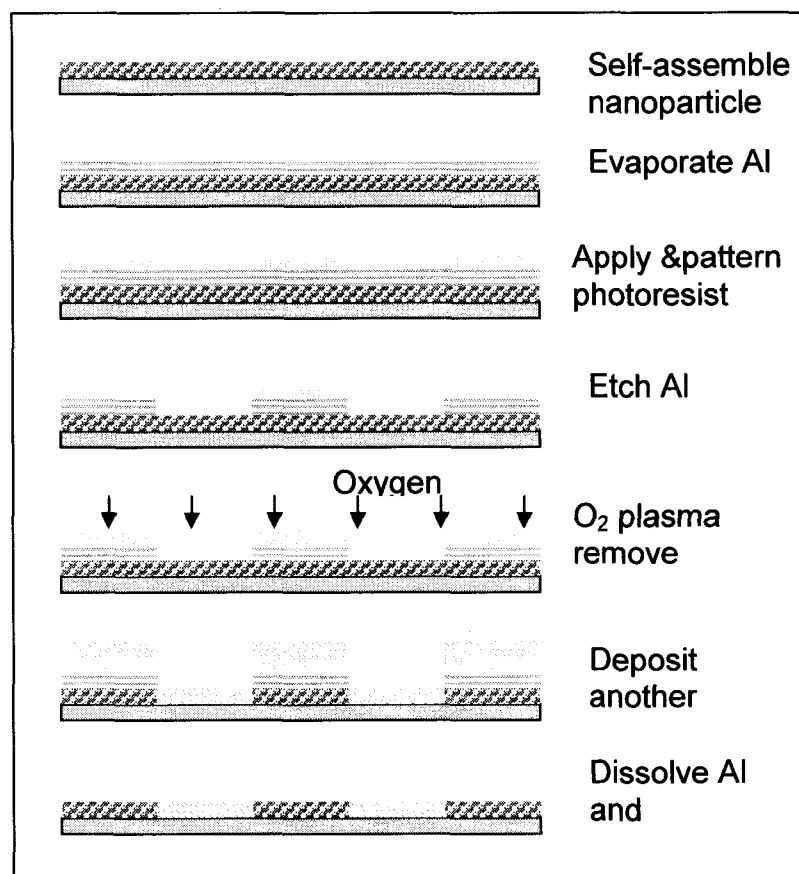
Fig. 2.6 Schematic of plasma method to pattern two type of nanoparticle on silicon wafer

As shown in SEM pictures, figure 2.7, clear patterns of 5 µm feature size were created with a sharp border between 78 nm silica and 150 nm polystyrene nanoparticles.

The upper left part is composed of 150 nm polystyrene nanoparticles and the lower right part is 78 nm silica nanoparticles. Fig. 2.7c was taken at the magnification of 30 k from which we can see that two types of particles are thoroughly separated by this method. UV light lithography, wet etching, dry etching and lift-off are all ordinary microelectronic processes. We can see that an optimized combination of them can offer us a strong capability to apply the conventional lithography to the LbL self-assembly nanotechnology. The high reproducibility of the process ensures that almost all the patterns on the 4 inch wafer are in similarly high quality.

However, because the LbL self-assembled nanoparticle films are unlike the conventional thin films in many respects, modification and optimization of the traditional process is required. Some issues during the process must be emphasized.

The drying step is critical for LbL self-assembled films. It can improve the adhesion and thickness of the films by enhancing the linkage between the materials that compose the film and removing the moisture. In the laboratory, the drying was realized with a nitrogen gun by hand. The random fashion of this operation often makes the films nonuniform over the broad area of wafer surface. An efficient way was found to use a spinner to spin off the water on the wafer surface. The rotation movement results in a much more uniform film which makes the subsequent process easier. The rotating speed is set at 1300 rpm, and a higher speed is not considered beneficial because it may drive the water drops away from the center too quickly so that the assembled materials will be carried away with them. Apparent radius traces created by liquid and solid flows can be observed on the wafer surface at higher rotating speed.

When the lift-off was executed, acetone was not used to dissolve photoresist, mainly because acetone was sometimes found to be detrimental to LbL assembled thin films although the damage is not so severe. In fact, the remaining resist was exposed again and later removed by developer solution. The developer is also able to etch aluminum at a lower but controllable rate. Therefore, it also works as the aluminum etchant after the photoresist is dissolved.

After the RIE dry etching of nanoparticle thin films, tiny scraps were observed sticking to the channel which was supposed to be a smooth and clean silicon surface. They must be removed prior to the next LbL self-assembly of silica nanoparticles and lift-off. Otherwise, the scraps may be dissolved from the surface during the lift-off and leave defects on the nanoparticle films. They can be removed after the wafer is shaken in an ultrasonic cleaner for 1 min.
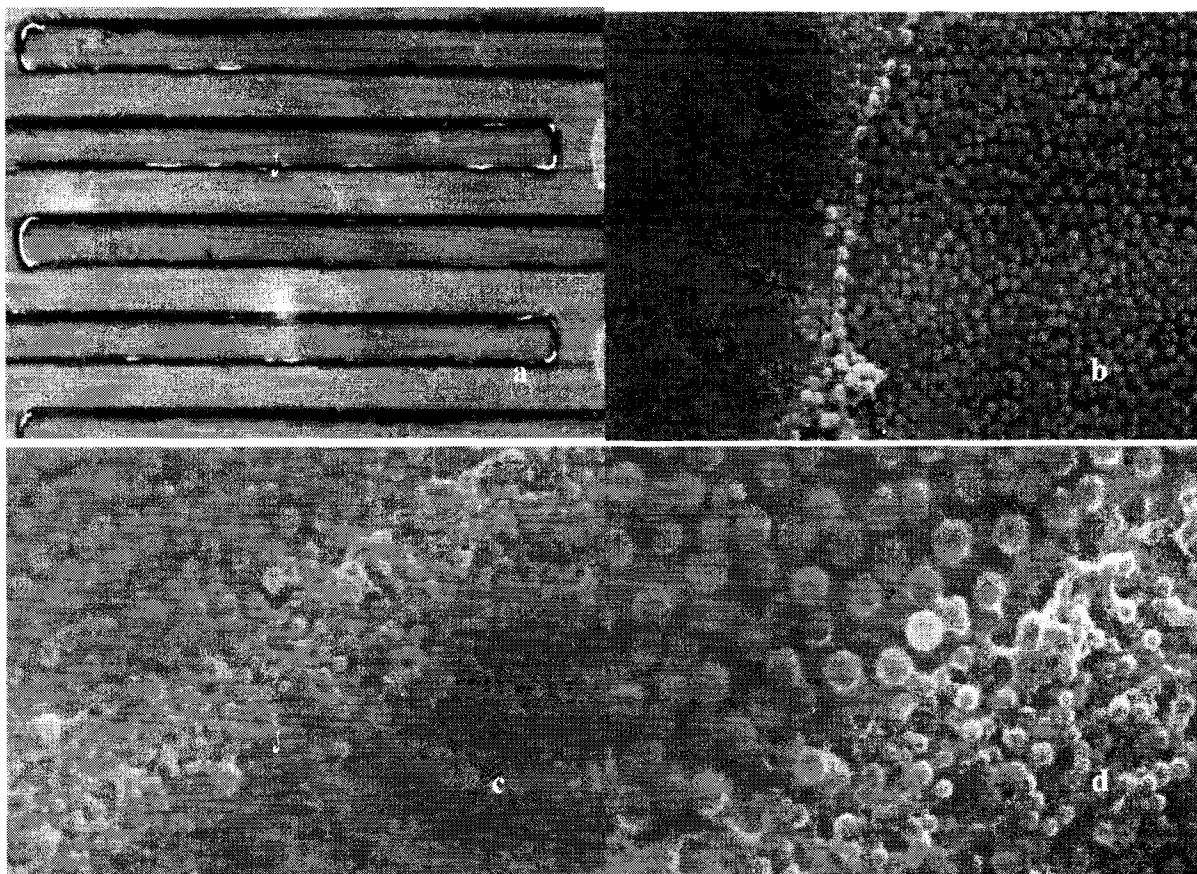
Fig. 2.7 SEM pictures of two types of patterned nanoparticle films: (a) Strips filled with 78 nm silica and 150 nm polystyrene nanoparticles alternately; (b)-(d) Magnified images of the interface between silica and polystyrene particles.

2.2.2. Two Lift-Off Method

The plasma method will employ expensive plasma equipment as well as introduce contamination in the structure. The two lift-off method is, therefore, developed to overcome this disadvantage. The nanoparticles used are carboxylate modified polystyrene particles, 150 nm and 64 nm in diameter, and were obtained from Seradyn Inc. They were diluted to 8 mg/ml.

Initially, the 4-inch silicon wafer was put into sulfuric acid and hydrogen peroxide solution (volume ratio 3:7) at 70°C for 1 hour. It was baked by a hotplate at 150°C for 3

min. The negative photoresist were dropped onto the wafer and spun at the speed of 1000 rpm for 40s. It was baked by the hotplate at 150°C again for 80 s. Then it was placed under a mask and exposed by the UV light irradiation for 26 s. It was baked by the hotplate at 100°C for 85 s and developed by its developer RD-6 for 12 s. At this point, the patterns on the mask have been transferred onto the resist.

The wafer was immersed in the PDDA, PSS and 150 nm polystyrene nanoparticle solutions alternately in a sequence of: [PDDA (10 min) + PSS (10 min)]$_2$ + [PDDA (10 min) + polystyrene (10 min)]$_3$. The intermediate rinsing (1 min in DI water) and drying steps must be involved to ensure a strong and clean film. Thin films of PDDA, PSS and polystyrene particles were adsorbed layer by layer by the electrostatic interaction because they were all oppositely charged. A layer of 900Å thick aluminum was evaporated onto the nanoparticle thin film after which 3 layers of 150 nm particles were coated once more in a sequence of [PDDA (10 min) + polystyrene (10 min)]$_3$. After that, another layer of 800Å thick aluminum was evaporated on. The wafer was put in the acetone solution to do the lift-off, during which ultrasonication was introduced to help remove the polyion thin films.

64 nm polystyrene nanoparticles were coated on the entire surface in a sequence of [PDDA (10 min) + PSS (10 min)]$_2$ + [PDDA (10 min) + polystyrene (10 min)]$_1$. Finally, the wafer was put into MF-319 solution (volume ratio 1: 6) to dissolve the aluminum and remove the smaller particles above it. Ultrasonication was necessary during the lift-off to remove the polyion and smaller nanoparticles. The schematic is shown in figure 2.8.
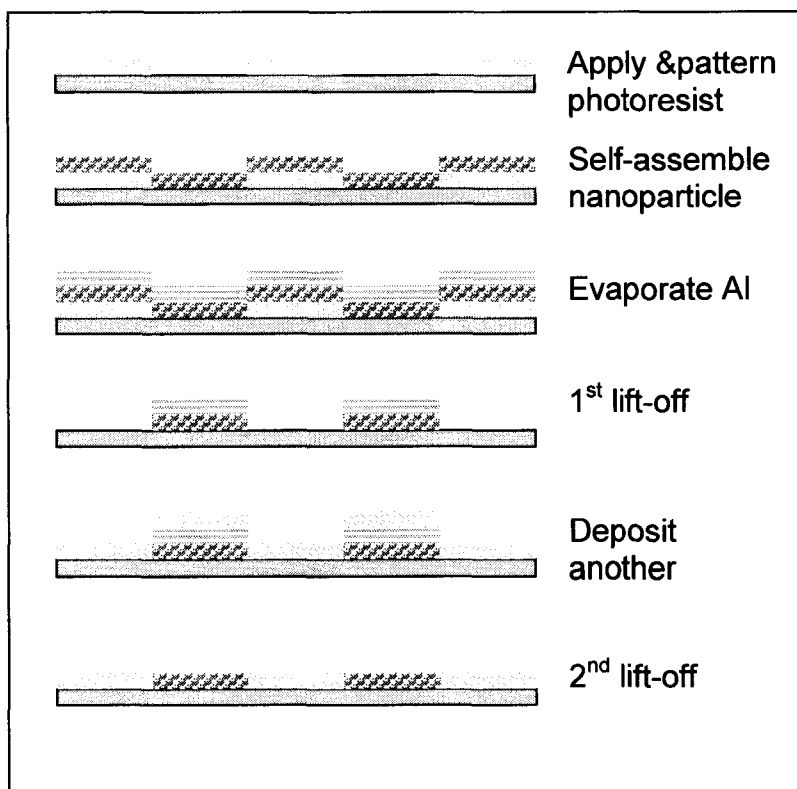
Fig. 2.8 Schematic of two lift-off method

As shown in figure 2.9, two types of nanoparticles, 64 nm and 150 nm polystyrene, were successfully settled in different regions as desired. The designed patterns consisted of regularly arranged squares with a side and distance of 5 μm. After the process, the 64 nm nanoparticles were filled into the tiny squares with 150 nm particles surrounding them.

The ultrasonication must be introduced during the lift-off to break the linkages among the polyion layers. The LbL self-assembled nanoparticle thin films are sandwiched between oppositely charged polyion films which could be regarded as a cross-linked net that is not readily cut off. They can not be removed when the materials

under them are dissolved. On the contrary, they tend to come down and reattach to the places the dissolved materials used to occupy. In this case, the nanoparticles between two polyion layers also can not be removed. The ultrasonication provides a way to break off the polyion net when the materials underneath are dissolved and completely lift off the nanoparticles.

The negative photoresist and aluminum were selected as the lift-off materials in this experiment. The photoresist is a common lift-off material. Of course, other substitutes can be selected instead of aluminum. MF-319 served as the aluminum solvent due to the slow dissolving rate that can put the dissolving under control.

The thickness of the aluminum is a factor that needs to be taken into consideration in the process. It is found that a thick aluminum layer may peel off many parts of the 150 nm nanoparticle films under it. On the other hand, a thin aluminum layer is not enough to lift off all 64 nm nanoparticles on it. Our solution is to split the aluminum into two layers and insert 3 layers of 150 nm nanoparticle films in between. As described in the experiment section, the first layer of aluminum deposited is 900 Å which is right above the 150 nm nanoparticle film. The second aluminum layer which is 800 Å in thickness is separated from the first layer by 3 layers of weakly attached 150 nm nanoparticle films. When the aluminum is being dissolved, the 900 Å aluminum can not peel off the 150 nm nanoparticle films, and a total thickness of 1700 Å can lift off the 64 nm nanoparticles completely.
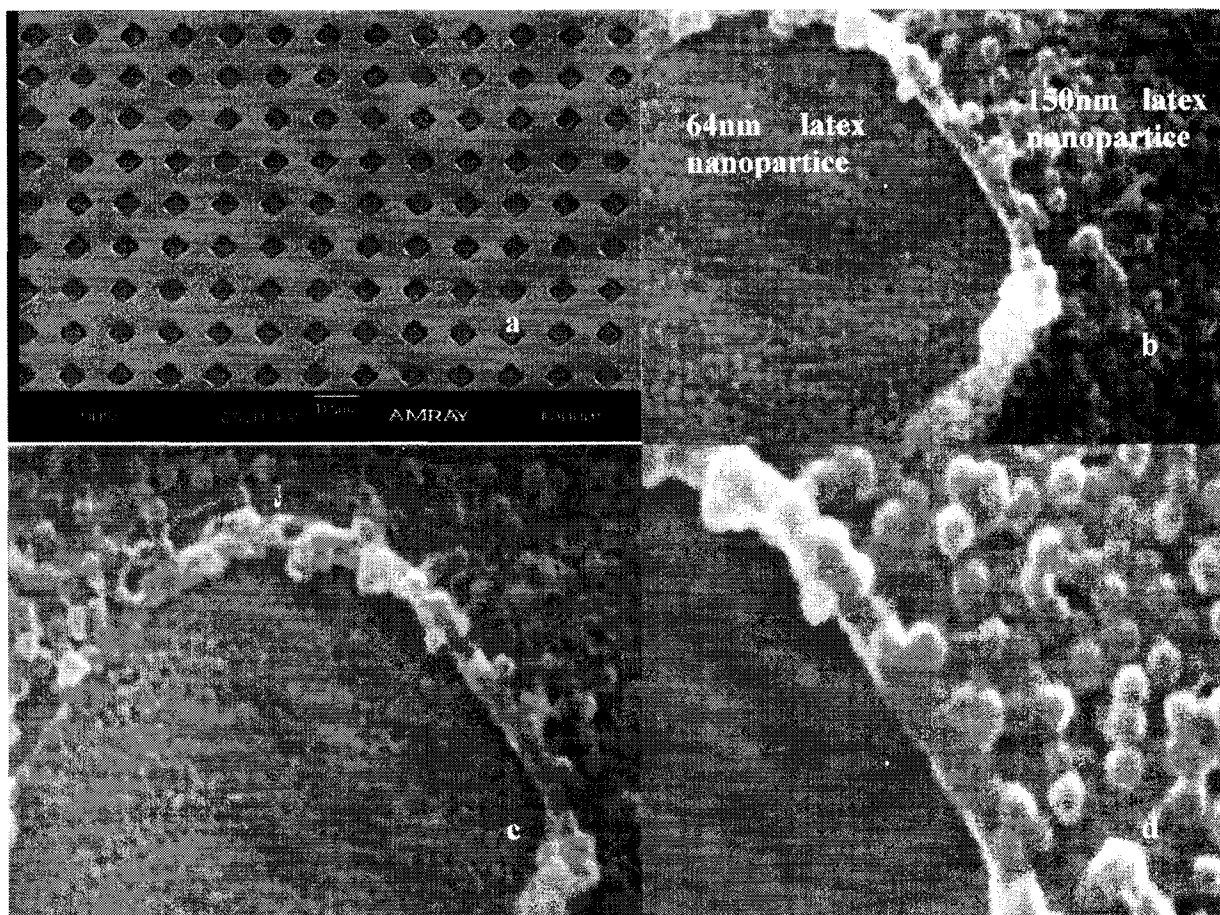
Fig. 2.9 Sem images of the spatial separation of two nanoparticles at different magnification (a) Matrix comprised of 5 μm squares, 64 nm nanoparticles were filled in the square and 150 nm ones surrounding them at 1k magnification (b, c) At 30 k (d) At 50 k

2.2.3. Analysis of the Thin Film

Before different nanoparticle thin film can be incorporated into the device, it must have a dense structure. In other words, the nanoparticle spheres must contact with each other very well; otherwise, it will not function properly in the device. In the situation where a perfect surface is necessary, for example when a 3D platform is to be built, this is the factor that must be taken into consideration. Any defect, such as a pinhole, also

needs to be avoided in order to prevent short-cut between top and bottom layers and enhance the conductivity of the conductive layers.

Thin film produced by our methods apparently has a dense structure which can be proved by the SEM image. Another way to prove this is to measure the surface roughness. The rms roughness and average roughness are defined by equations

$$R_q = [\frac{1}{L} \int_0^L Z^2(x)dx]^{1/2}$$

and

$$R_a = \frac{1}{L} \int_0^L |Z(x)| dx$$

where Z(x) is the difference of surface coordinate and the mean value.

As shown in Fig. 2.10, if the spherical particles are all uniformly coated and closely packed, the surface is composed of continuous half circles and the roughness should approximate one fourth of the diameter in theory. In our experiment, we selected 300 nm nanoparticle, so the surface roughness should be 75 nm.
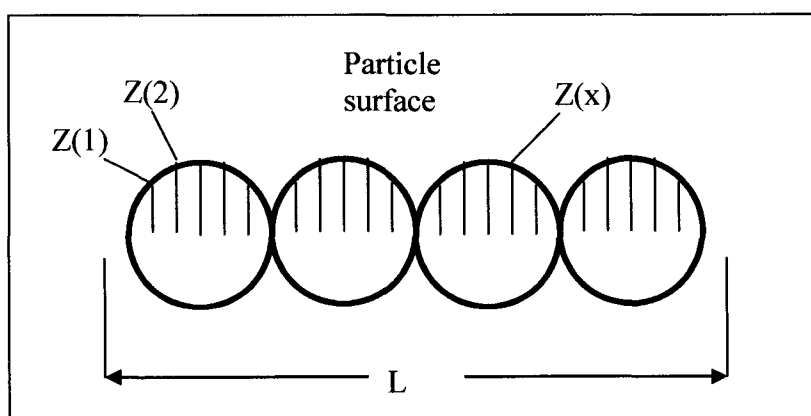
Fig. 2.10 Surface roughness profile Z(x)

Our experimental results, 87 nm and 74 nm which are corresponding to modified lift-off and metal-mask method respectively, agree with it and imply a closely packed layered structure. In Fig. 2.11, the 3-D plot and surface roughness of the created U-turn pattern are shown.

To some extent, the roughness might be reduced by using smaller particles. But on the other hand, smaller particles usually have a wider size distribution which may result in more serious irregularity. Higher concentration of particle solution is recommended. In addition, the thickness of metal mask can be a little larger to keep the particles layer from damage during etching process.
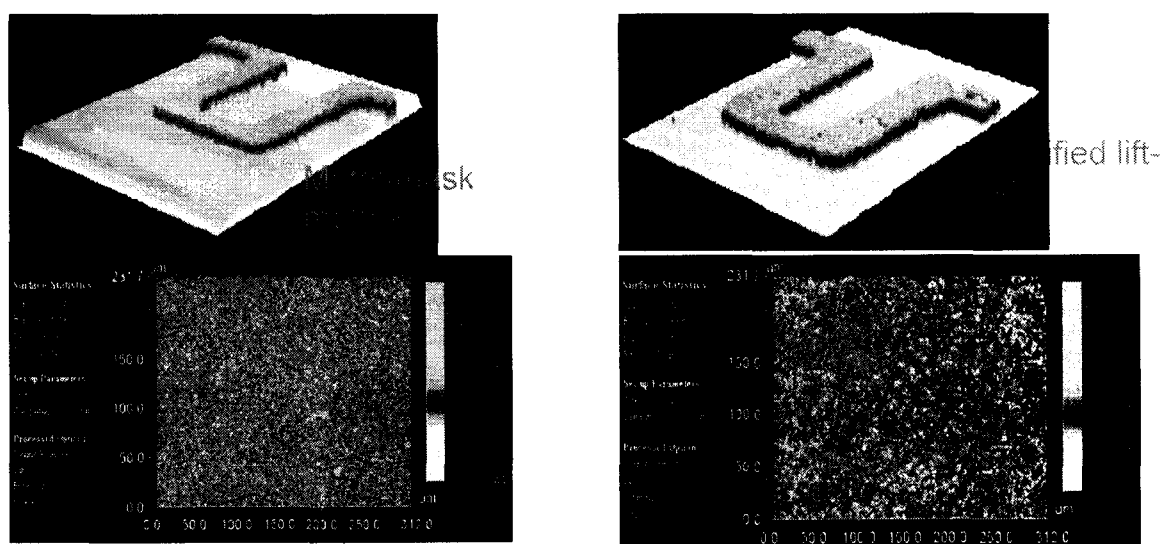
Fig. 2.11 Surface characteristics measured by a Wyko RST interferometric microscope (top) 3D-image of a U-turn pattern 20-μm in width which is made of 300 nm nanoparticle/PDDA multilayer. Blue is multilayer and yellow is silicon bare surface. (Bottom) The multilayer surface roughness.

CHAPTER III

THIN FILM FABRICATED BY LbL SELF-ASSEMBLY

Thin films composed of different functional substances must be discovered which can be layer-by-layer self-assembled onto the silicon wafer and function in the device. There are a lot of candidates for thin film fabrication because many suppliers are available to provide with various nanoparticle dispersions or powders in a variety of sizes. After purchasing and making a solution of the nanoparticle, we used zeta potential analyzer, QCM and SEM to analyze the thin film.

3.1. Zeta Potential Analyzer

The physical properties of colloids and suspensions are strongly dependent on the nature and extent of the particle-liquid interface, the behavior of aqueous dispersions being especially sensitive to the electrical and ionic structure of the interface. The production and stability of colloids and suspensions are both intimately related to the so-called electrical double layer that characterizes the interface. Almost all particulate or macroscopic materials in contact with a liquid acquire an electronic charge on their surfaces. Zeta potential is an important and useful indicator of this charge which can, for example, be used to predict and control the stability of colloidal suspensions or emulsions. The greater the zeta potential the more likely the suspension is to be stable

48

because the charged particles repel one another and thus overcome the natural tendency to aggregate. The measurement of zeta potential is often the key to understanding dispersion and aggregation processes in applications as diverse as water purification, ceramic slip casting and the formulation of paints, inks and cosmetics. Zeta potential can also be a controlling parameter in processes such as adhesion, surface coating, filtration, lubrication and corrosion. Consequently, the presence or absence of charged groups on the surface of macroscopic materials such as hair, glass fiber, paper pulp, plastic films and refractories, as revealed by their zeta potentials can directly affect their performance and processing characteristics. Brookhaven offers you a choice of instruments to meet your needs in each of these fields.

Information relating to stability is therefore of considerable importance. It should be noted that the term stability, when applied to colloidal dispersions, is generally relative in meaning and intended to express the resistance to change of the dispersion with time. Zeta potential measurements are directly related to the nature and structure of the electric double layer at the particle-liquid interface.

The most important factor that affects zeta potential is pH. A zeta potential value quoted without a definition of it's environment (pH, ionic strength, concentration of any additives) is a meaningless number.

Imagine a particle in suspension with a negative zeta potential. If more alkali is added to this suspension then the particles tend to acquire more negative charge. If acid is added to this suspension then a point will be reached where the charge will be neutralized. Further addition of acid will cause a build up of positive charge. In general, a zeta potential versus pH curve will be positive at low pH and lower or negative at high pH.

There may be a point where the curve passes through zero zeta potential. This point is called the isoelectric point and is very important from a position of practical consideration, as shown in figure 3.1. It is normally the point where the colloidal system is least stable. When stability is an important factor in the colloidal process, zeta potential measurements are necessary.
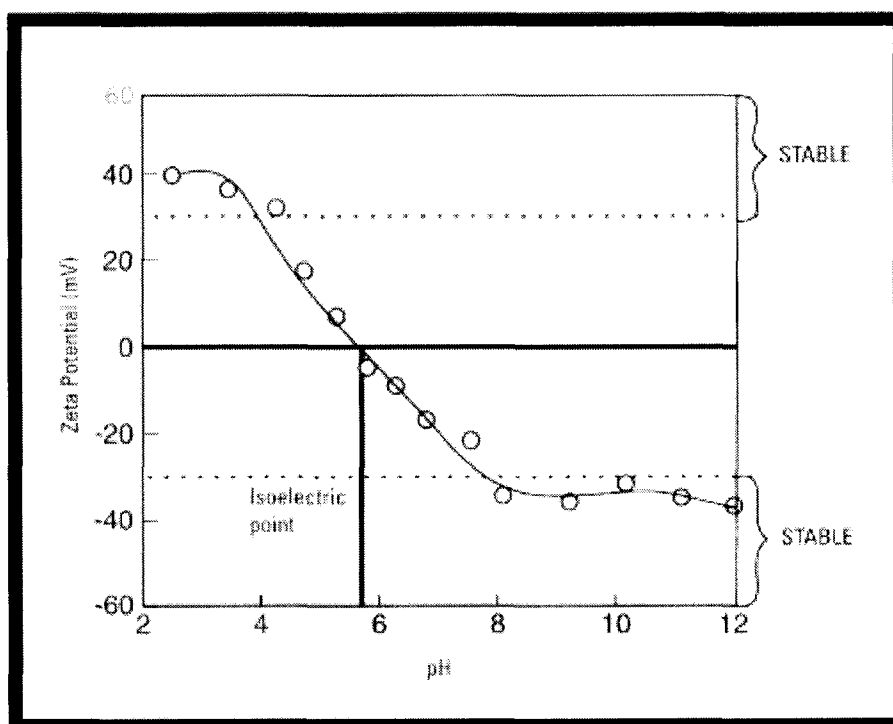
Figure 3.1 Zeta potential vs. PH.

Some of the applications in layer-by-layer self-assembly are: the measurement of the nanoparticle size, the polarity and amount of the surface charge. For example, as shown in the below graph, the zeta potential of In2O3 nanoparticle is 47 mv, meaning it is positively charged. If it needs to be coated on a silicon wafer with layer-by-layer self-

assembly, a negative polyion, such as PSS is recommended to be alternately adsorbed with it.

indium oxide (Run 10)
Measurement Completed

Power	1.0 / 0.5 / 0.0

Frequency Shift (Hz)
-150   0   150

Zoom   Frequency Shift   Run 10

Zeta Potential

Run	Zeta Potential (mV)	Half Width (mV)
1	59.36	1.98
2	51.57	2.08
3	45.12	2.07
4	63.30	1.98
5	53.04	2.07
6	33.81	3.54
7	27.93	2.00
8	39.83	1.90
9	45.21	1.74
10	52.80	1.95
Mean	47.80	2.13
Std. Error	3.29	0.16

Measurement Parameters:

Conductance	= 0 μS
Current	= 0.14 mA
Electric Field	= 23.15 V/cm
Sample Count Rate	= 240 kcps
Ref. Count Rate	= 2582 kcps

Start   Runs   Hide Graph

Clear   Parameters   Copy To Clipboard

Figure 3.2 Zeta potential of In_2O_3

3.2. QCM

QCM equipment produced by USI System in Japan was used to monitor the assembly process. The resonators used were covered by evaporated silver electrodes on both sides. The resonance frequency was 9 MHz (AT-cut). The QCM resonator was immersed for a given period of time in a polyelectrolyte solution and dried in a nitrogen

stream. The frequency changes were then measured. All experiments were carried out in an air-conditioned room at about 22 °C.

As mentioned in the previous chapter, QCM is a microbalance suitable to detect the tiny mass and thickness adsorbed on its face. It senses the resonance frequency directly which results in a high sensitivity. The frequency decrease can be converted to an increment of adsorbed mass and thickness as the following equations by taking into account the characteristics of quartz resonators, so the prefactors are specific to the system.

$$\Delta F \text{ (Hz)} = -1.83 \times 108(\text{Hz cm2/g}) \, \Delta M \text{ (g)}/A \text{ (cm2)} \qquad (1)$$

where M (g) is the adsorbed mass, ΔF (Hz) is the frequency shift and A is the apparent area of quartz microbalance placed between QCM electrodes. This is 0.16 ± 0.01 cm2 in our system. Then, one finds that 1 Hz change in ΔF corresponds to 0.9 ng in weight. The thickness of the alternate layer corresponding to QCM frequency shift was dete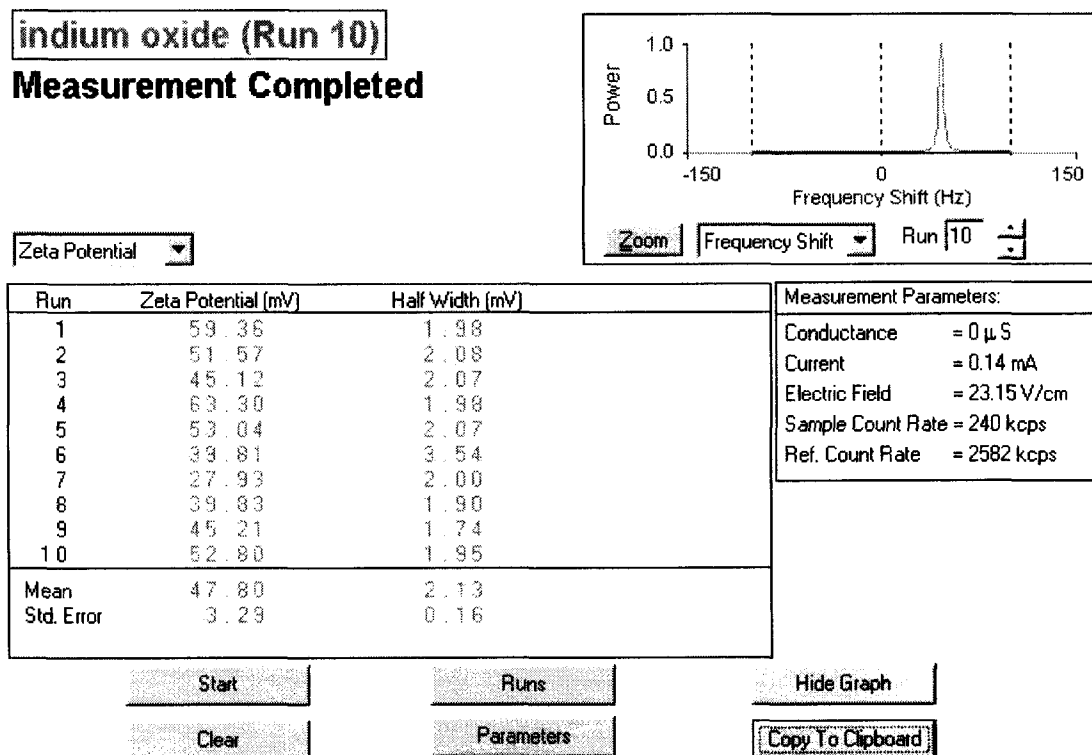rmined by observation of the film cross-section from SEM images of cut resonators coated with silicon/polycation films, which gives the following relationship with ±5 % error:

$$d \text{ (nm)} = -0.022(\text{nm/Hz}) \, x\Delta F(\text{Hz}) \qquad (2)$$

In the first stage, a well-defined precursor film with a thickness of about 10 nm was assembled from PDDA and PSS onto resonators or mica. The precursor films contained 3 polyion layers in the alternate mode: PDDA /PSS, and the terminal layer were "positive" PDDA. Then a substrate was alternately immersed for 15 min in aqueous dispersions of In_2O_3 and in aqueous PSS with intermediate water washing. This process was periodically interrupted for the purpose of measuring QCM resonance frequency.

Figure 3.3 shows the growth of In$_2$O$_3$/PSS multilayer on the substrate. The first 5 steps

represent the precursor layer. Next the bigger leap represents the nanoparticle growth and

smaller one represents the polyelectrolyte because the molecular weight and size of

nanoparticle are bigger than polyelectrolyte. After the production of nanoparticle thin

film on wafer, the sample must be observed under SEM or AFM to make sure it has a

dense structure, as shown in figure 3.4 which is a dense SnO$_2$ nanoparticle structure.
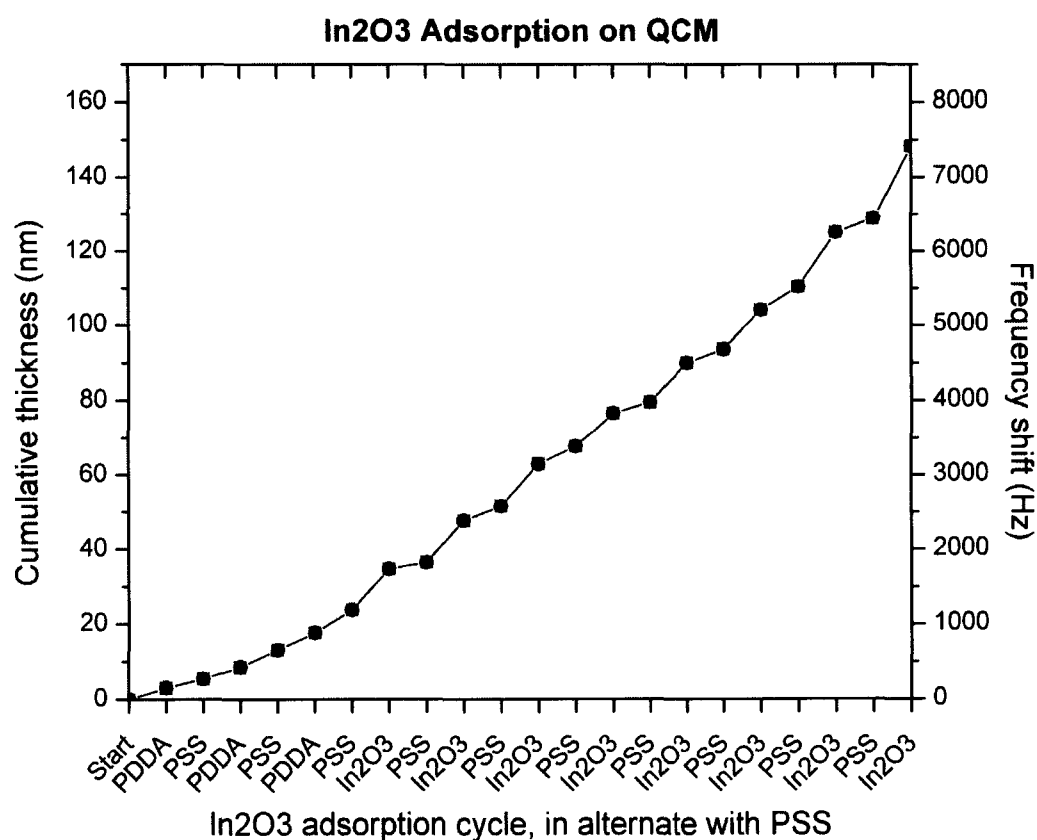
Figure 3.3 In$_2$O$_3$ nanoparticle growths on substrate
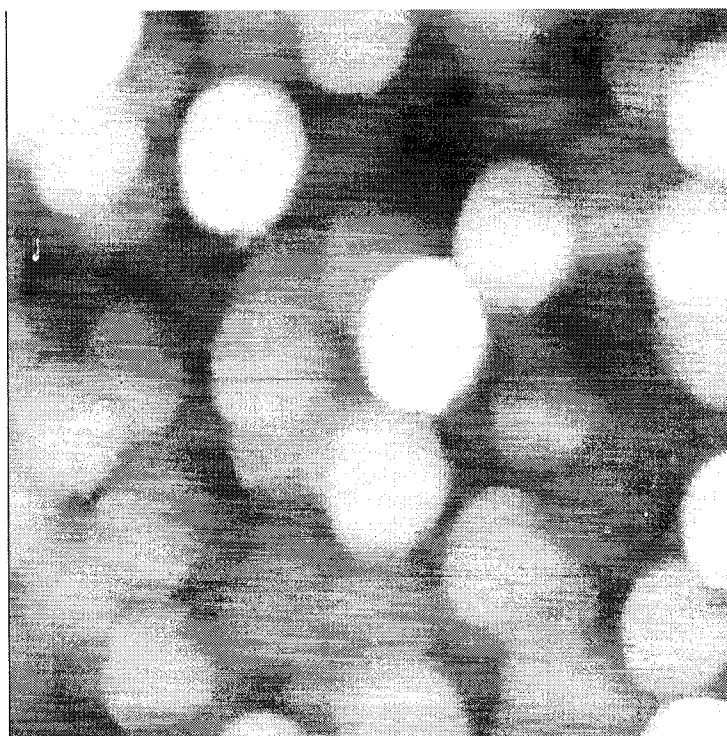
Figure 3.4 AFM image of SnO$_2$ nanoparticle thin film

CHAPTER IV

MOS-CAPACITOR

4.2   Fabrication &Structure

Metal-oxide-semiconductor capacitor arrays are fabricated on both P and N type

silicon wafers using layer-by-layer self-assembled insulating layers.   The vertical

dimension of the self-assembled thin film can be precisely controlled as well as the

molecular order.   Unlike the conventional process, the layer-by-layer self-assembly

allows one to obtain the thin films for a semiconductor device with a dramatically lower

temperature, lower cost and shorter processing time. The deposited thin film is stable and

can grow on any substrate other than silicon. The conventional lithographic technique is

employed to pattern the self-assembled thin films, resulting in an extremely high

reproducibility. This enables the possibility of industrial applications to fabricate devices

with this simplified and versatile technique.

These capacitors can be fabricated onto integrated circuit chips.   Metal-oxide-

semiconductor (MOS) capacitors, with thermal SiO_2 as the gate oxide, have become the

prime structure to carry out digital functions in silicon integrated circuits. However, the

fabrication of a MOS capacitor using the conventional silicon MOS technology demands

sophisticated facilities. High process temperature also needs to be balanced to avoid the

damage to subsequent processes. And, the growth rate of the thermal silicon dioxide is

55

usually very low. Hereby, an approach to fabricate the basic MOS capacitor with a technique combining traditional lithographic technique and LbL self-assembly was developed because a dielectric layer consisting of silica and polyion can be self-assembled easily and rapidly. The insulating layer is made of 6 layers of LbL self-assembled silica nanoparticle thin film. Capacitors are fabricated on 4 inch P-type and N-type silicon wafers. Aluminum is evaporated on the top as the electrode. The measured CV curves are in compliance with typical MOS capacitors. Compared to the traditional process, this has the advantages of low temperature, low cost, and short processing time. LbL self-assembly is also called molecular beaker epitaxy because it only requires several beakers to realize the "dipping in" adsorption. The lithographic technique is already a mature process, widely used in the microelectronic industry. The combination of traditional lithography and LbL self-assembly guarantees an extremely high reproducibility in fabrication of semiconductor devices. The regular dipping also enables the automation of this process if it is applied to mass production. The self-assembled thin film of silica nanoparticle is stable enough to withstand the ultrasonic wave. The simplicity and reliability of this process to fabricate the simple MOS capacitor provides a new way to fabricate other microelectronic or optoelectronic devices by traditional lithography and LbL self-assembled building blocks.

Materials: Poly (diallyldimethylammonium chloride), MW 200-300K (PDDA, Aldrich), and sodium poly (styrenesulfonate), MW 70,000 (PSS, Aldrich), were commercially available and used without further purification at a concentration of 1.5 - 3 mg/mL. The pH of the solutions was adjusted by adding aqueous NaOH or HCl. PDDA is a quarternary ammonium linear polycation and PSS (pKa 1) is a linear polyanion.

Polyions were used in solutions at pH 8. SiO2 colloidal solutions (231 mg/mL, Nissan

Chemical, Ltd) were diluted in water to provide concentrations of 10 mg/mL at pH 9.

The diameter of the silica particles was 45 ± 5 nm. The substrates were 4-inch silicon

(a)

(b)

(c)

(d)
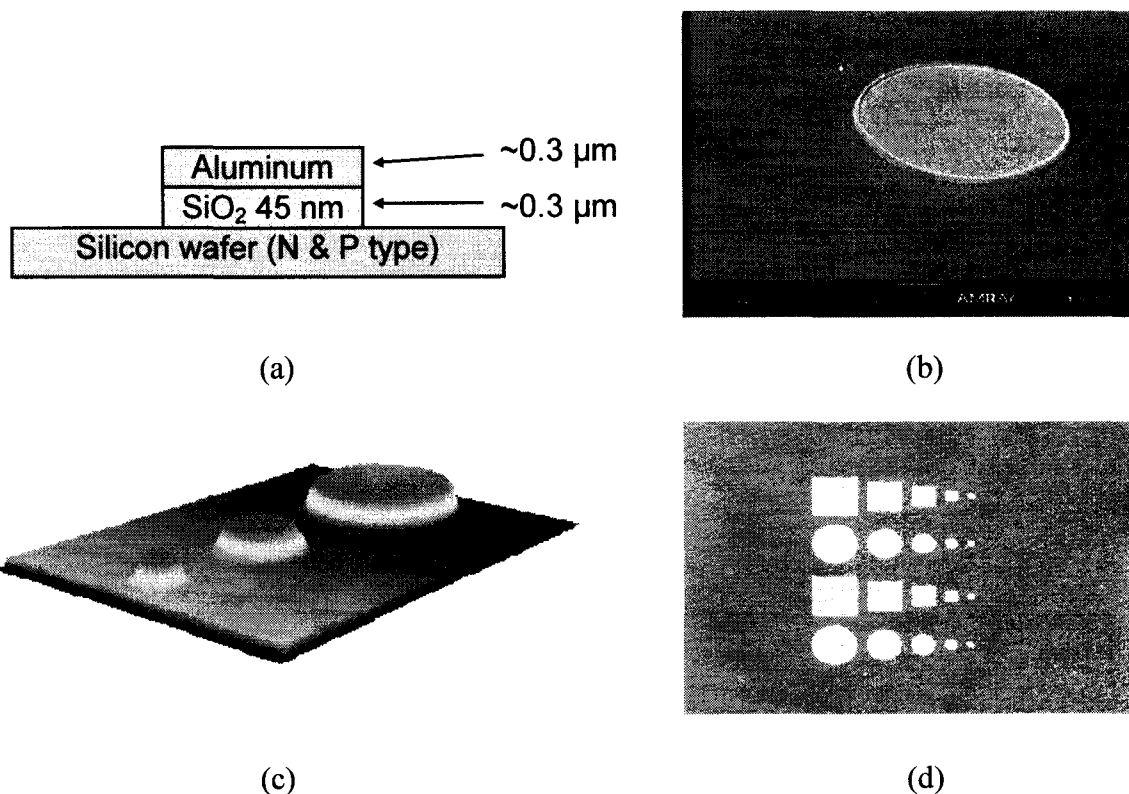
Figure 4.1 (a) Structure of the MOS-capacitor, (b) A single capacitor on silicon wafer (c-d) Arrays of capacitor

wafers, P type (orientation <100>, > 1 OHM-CM) and N-type (orientation <100>, 1-100

OHM-CM) from Silicon Quest Inc. A double-side mask aligner (EV420 from Electronic

Visions, Inc.) was used as the UV light illuminator. Aluminum layers were deposited on

a silicon substrate by the DV-502A high-vacuum evaporator from Denton Vacuum, Inc.

The WYK RST white light interferometer microscope was used to measure the surface roughness and dimension of the thin film. The electronic characteristic instrument was from Keithley Co., Inc. Ultrasonication was performed with an 8892 Cole-Parmer ultrasonic cleaner. A CCD camera was used to produce the image of the pattern, and a white light interferometric microscope was used to measure the dimension and surface roughness of the produced device. The quartz crystal microbalance served to monitor the growth of the self-assembled thin films.

Initially, the 4-inch silicon wafer was put into sulfuric acid and hydrogen peroxide solution (volume ratio 3:7) at 70°C for 1 hour. The wafer was completely rinsed by DI water and baked on a hotplate at 150°C for 5 minutes to remove the moisture. Then it was placed on a spinner to coat a layer of negative photoresist (NR9-1500P from Futurrex, Inc.). The maximum speed was set at 1000 rpm for 40 seconds. The wafer with photoresist was baked on a hotplate at 150°C for 80 seconds. The resist was subsequently exposed by UV light for 22 seconds to transfer the pattern from the mask onto the resist. Next, it was baked at 100°C for 80 seconds and finally immersed in developer solution for 12 seconds. At this point, the capacitor pattern was transferred onto the resist.

Following the above steps, LbL assembly of 45 nm silica particles was implemented on the silicon wafer. The sequence of the alternate immersion was [PDDA (10 min) + PSS (10 min)] 2 + [PDDA (10 min) + silica (10 min)] 6. The intermediate rinsing and drying after each immersion was necessary. The rinsing was done by purging the wafer in DI water flow for 1 minute. The wafer was placed on a spinner and spun to remove water by centrifugal force. The maximum rotation speed was set at 1300 rpm for

a time of 45 seconds. Subsequently, the deposition of aluminum was carried out at a pressure of 10-5 mtorr with a deposition rate of 2 Å/s until a thickness of 3000 Å was reached. The wafer was then soaked into acetone solution for 5 minutes to dissolve the photoresist, and an ultrasonic bath was introduced for roughly 3 seconds to improve the lift-off.

The capacitors were made on both P and N type wafers. The capacitance versus voltage curves were obtained under a voltage range from -2V to 2V with a step of 20 mV.

Figure 4.2 shows an SEM image of the growth of (45-nm silica/PDDA) the multilayer including 4 and 10 multilayer cross-sections. The film has a permanent thickness of 170 nm, leading to 43 nm for every bilayer close to the silica particle diameter. A film mass from QCM and film thickness from SEM gives a density of the SiO_2/PDDA multilayers as $\rho = 1.43 \pm 0.05$ g/cm3. To calculate the silica packing coefficient in the films, it is reasonable to assume that the dry film consists of SiO_2, PDDA, and air-filled pores. The mass ratio of PDDA to PDDA/SiO_2 bilayer obtained from QCM measurements is 0.08. Given the component densities ($\rho = 1.43$, $\rho_{SiO2} = 2.2$, and $\rho_{PDDA} = 1.1$ g/cm3), the volume ratio is obtained as $V_{PDDA}/V_{bilayer} = 0.1$. From the equation

$$\rho_{PDDA}V_{PDDA} + \rho_{SiO2}V_{SiO2} + \rho_{air}V_{air} = \rho V \qquad (3)$$

where the air-term is very small, V_{SiO2}/V is figured out to be 0.7. This is very close to the theoretical dense-packing coefficient for spheres (0.63), and corresponds to details in the SEM-micrographs. SiO_2/PDDA film volume composition is: 70 % SiO_2 + 10 % polycation + 20 % air-filled pores. These pores are formed by closely packed 45-nm SiO_2 and have a typical dimension of 15 nm. Therefore, the dielectric constant of our

silica/PDDA multilayer is different from silica due to about 30% of inclusions, such as
air, polyion layers, etc. In the analysis of the MOS devices, it is found that the dielectric
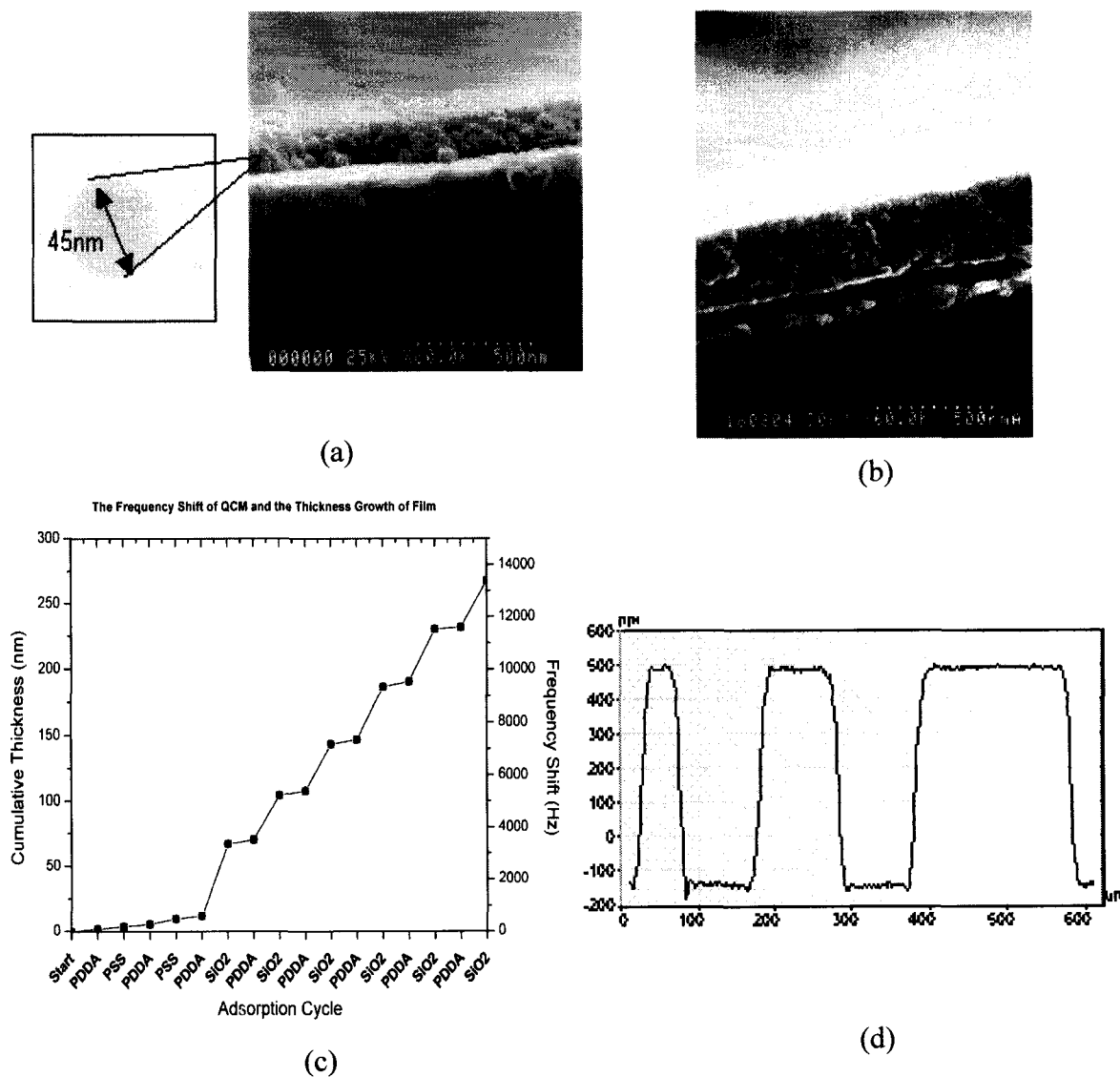constant was

(a)

(b)

(c)

(d)

Figure 4.2 (a-b) SEM images of silica nanoparticle growth on substrate. (c) QCM
monitoring silica growth on surface. (d) Thickness of real device

slightly higher than the one for thermal silica. In our group, it is possible to produce ultrathin multilayers of silica nanoparticles in the thickness ranging from 100 nm to hundreds of nm with precision of about 10 nm. These films have a porous structure related to the close packing of silica spheres in the layer.

As shown in Figure 4.1, clear patterns of the capacitor arrays with sharp borders were created on a silicon wafer. The arrays consist of round and square capacitors with various sizes. All 45 nm SiO_2 spheres were closely packed to form a dense structure. The surface roughness of the capacitor was 6.5 nm measured by roughness-step-tester (RST). The growth step can be easily estimated by measuring the frequency shift of the quartz crystal microbalance resonator, and the monolayer thickness can be calculated accordingly by the Sauerbrey equation. Figure 4.2 gives the QCM monitoring of alternate PDDA and SiO_2 adsorption where the thickness was calculated from frequency shifts with formula 2. As recorded by QCM, at every assembly step, the component monolayer was formed. It shows that at the last cycle, the thickness of the SiO_2 layers is 260 nm. When added to the 300 nm aluminum electrode, the height of the whole device is 567 nm, well in compliance with the 2-D profile of Figure 4.2.

4.2 Electronic Characteristics

The fabricated device demonstrates the C-V curve of a typical MOS capacitor with distinct accumulation, depletion, and inversion regions, as shown in figure 4.3. The MOS structure is basically a capacitor with the silica as the dielectric material. If the silicon were a perfect conductor, the parallel-plate capacitance would be determined by the oxide capacitance as it is in the accumulation region. However, it always deviates from the oxide capacitance due to the voltage dependence of the surface space-charge

layer in silicon. The space-charge occurring at the interface of silicon and oxide acts as another capacitance in series with the oxide capacitor, giving an overall capacitance that is smaller than the pure oxide capacitance. Since the inversion of a P-type MOS capacitor happens at a positive voltage and an N-type one at a negative voltage, the C-V curves move in opposite directions for P and N type MOS capacitors. If the layer of silicon dioxide was produced by conventional thermal oxidation, the dielectric constant would be 3.9. Given the size of each square device 200 μm by 200 μm and 267 nm high, the oxide capacitance is calculated as 5.2 pF, reasonably close to the experimental data, 8 pF. The slightly larger value means a larger dielectric constant of the LbL self-assembled insulator layer. The precursor and intermediate polyion multilayer is the root for the higher dielectric constant because the dielectric constant of the polyion films is normally ten times higher than silica, as shown in table 4.1. The experimental results also show that the capacitance of each device is strictly proportional to the area of electrode, implying an extremely high reproducibility of the processes. The leakage current is hardly measurable in the testing system. Another important parameter, the flatband voltage VFB≈ -0.2~-0.5 v, can be extracted from fig. 4 by observing the turning point of depletion and accumulation region.

The process will take about 5.5 hours including 1 hr of cleaning, 1 hr of lithography and 3.5 hr of LbL self-assembly. In our process, a conventional lithographic technique, such as lift-off, was used to pattern the capacitors on multilayer films. However, because the LbL self-assembled nanoparticle films are unlike the conventional thin films in many respects, modification and optimization of the traditional process is required.

Other dielectric materials such as montmorillonite were tested as the insulating layer. They did not perform as well as the silica nanoparticle although the monolayer thickness can be more precisely controlled. There are many other nanoparticles suitable for LbL self-assembly which may function differently for various devices.

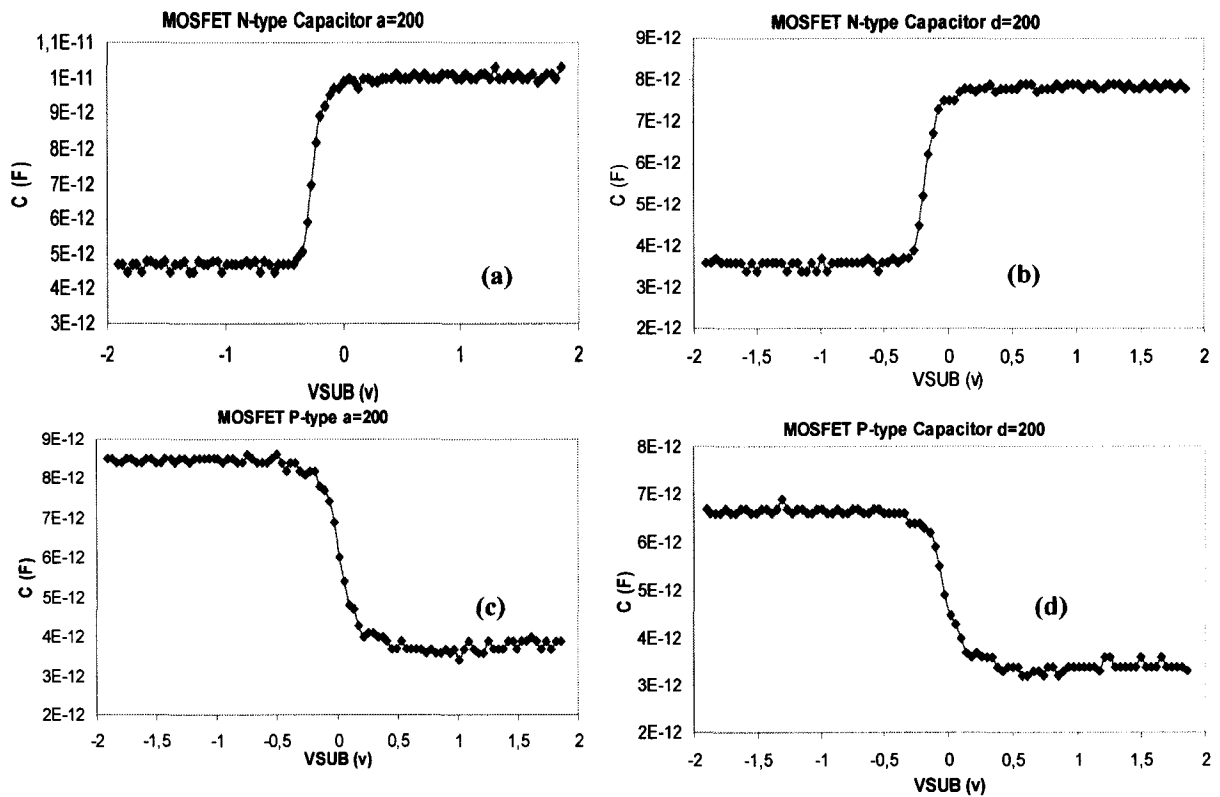| film type	Py-values[a]	ϵ
Qz/PEI/[PSS/PEI]₄	1.54 ± 0.05	30 ± 10
Qz/PEI/[PSS/PAH]₄	1.75 ± 0.06	50 ± 10
Qz/PEI/[PSS/PDADMAC]₄	2.22 ± 0.08	120?
Qz/PEI/[PSS/PAH]₂/[PAA-MePY/PAH]₁	1.89± 0.04	65 ± 10

Table 4.1 Dielectric constant of polyion multilayer

Fig. 4.3 Capacitance versus voltage curves of MOS P and N type capacitors (a) N type square capacitor with size of 200 μm (b) N type round capacitor with diameter of 200 μm (c) P type square capacitor with size of 200 μm (d) P type round capacitor with diameter of 200 μm

CHAPTER V

MOSFET

5.1.   Fabrication &Structure

In the previous chapter, the fabrication and characterization of a MOS capacitor is reported whose insulating layer was realized by the assembly of 6 layers of 45-nm silica (totally about 240 nm thick). The precision of the geometrical sizes of the device was 1 nm in the vertical direction and 1 μm in the plane. Its electronic characteristics were reliable, showing distinct accumulation, depletion, and inversion regions in the C-V curve. This proves that the LbL self-assembled silica nanoparticle thin film can operate in devices in the same way as the silicon dioxide by conventional thermal oxidation. The dielectric constant of this silica thin film was 6, which is higher than 3.9 for the conventional silicon dioxide because the charged polymers twisted between any two layers of nanoparticles has a dielectric constant ten times higher.

Based on the above results, we selected the 45-nm silica particles as the dielectric material for the MOSFET. In this work, 15-nm diameter SnO_2 and 45-nm diameter SiO_2 nanoparticles, constituting the semiconductive and insulating thin films, were patterned by the conventional lithography and lift-off processes. A patterned layer of titanium 90 nm thick serves as the source and drain electrodes, and another patterned layer of

65

aluminum 200 nm thick as the gate. The channel between the source and the drain is 100 μm wide and 3-5 μm long and is filled with 15-nm diameter Silica particles (Fig. 5.1).

Since both lithography and LbL nanoassembly are well-established techniques, the fabricated MOSFETs were reliable, and their electronic characteristics were highly reproducible. The thickness of the adsorbed nanoparticle multilayers was adjusted with the precision of a few nanometers. The only equipment required for nanoassembly was Dipping Automate (Rigler & Kirstein, Germany), and the process was carried out by alternate immersions of the wafer into two beakers containing nanoparticle and polycation solutions at room temperature. The reliability, simplicity, and versatility of the newly developed process provide a way to the potential commercialization of the approach combining microlithography with LbL nanoassembly.

The procedures of the MOSFET fabrication are described as follows. Initially, a 4-inch silicon wafer with a thin layer of thermal oxide is soaked in sulfuric acid and hydrogen peroxide solution (volume ratio 3:7) at 70 °C for 1 hour. Titanium is selected as the source and drain electrodes. A layer of Ti is sputtered onto the wafer and patterned by first lithography. Next, photoresist is spin-cast on the wafer. The second lithography is done by aligning the mask with the wafer to generate a window right above the channel region. The wafer is alternately immersed in aqueous poly (dimethyldiallyl ammonium chloride) (PDDA, MW 200,000, Sigma) and sodium poly (styrenesulfonate) (PSS, MW 70,000, Sigma) at a concentration of 3 mg/mL and pH 8, in a sequence of [PDDA (10 min) + PSS (10 min)]$_2$. Between the two immersions, there was an intermediate rinsing by deionizer water for 1 minute followed by spin drying the wafer at 1300 rpm for 40 seconds. These four layers of polyion films enhanced the subsequent nanoparticle

adsorption because they form a uniform and strongly charged 3-nm thick precursor on the wafer surface. Following it, 15-nm SnO_2 and 45-nm SiO_2 nanoparticles, taken at 8 mg/mL and pH 8 water dispersion (30), were coated on the entire surface of the wafer in the sequence [PDDA (10 min) + SnO_2 (10 min)]6 + [PDDA (10 min) + SiO_2 (4 min)]6 to produce an organized "sandwich" of semiconducting and insulating nanoparticles. A layer of aluminum 200 nm thick was evaporated on the surface. Finally, the wafer is soaked in acetone solution to perform the lift-off with sonication for 1 minute to cut off the links between polyions and to remove the materials above the photoresist everywhere except the gate region. The total device processing time was eight hours, and thousands of elements in parallel can be fabricated at one time.
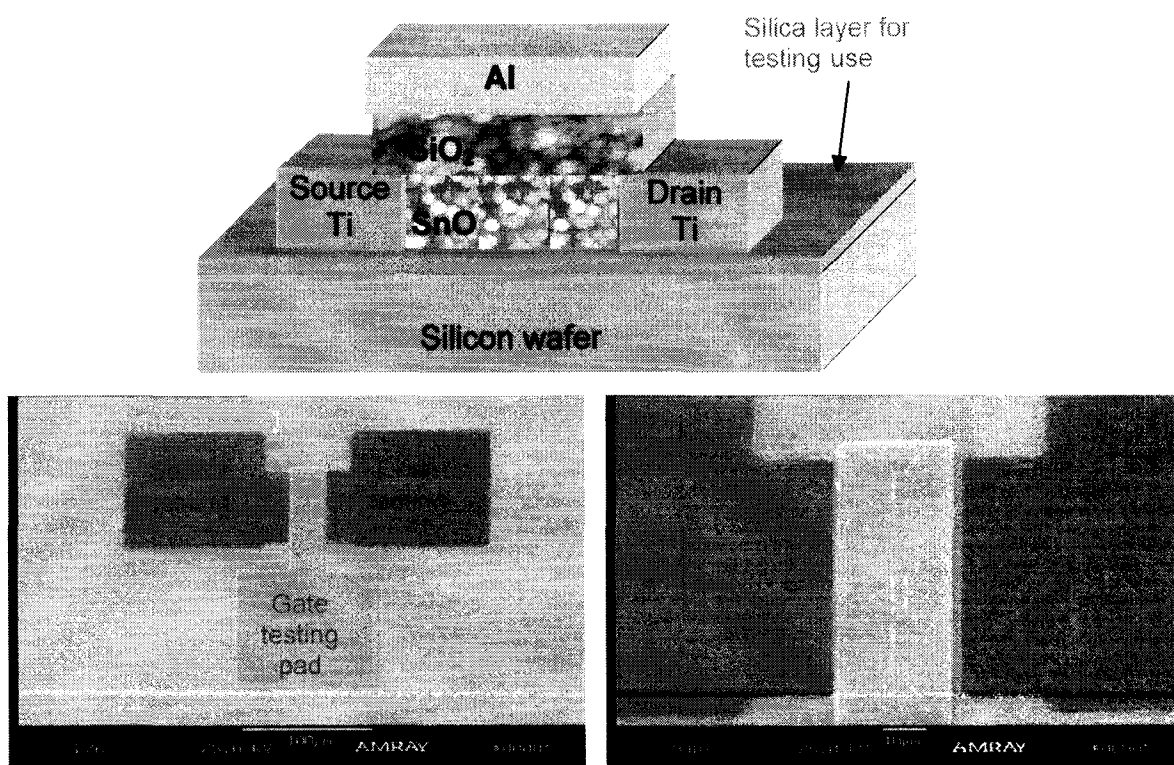

Fig. 5.1 (Bottom) Scanning electron microscopy (Amray) image of a MOSFET and amplified channel region. (top view). (Top) Structural schematic of the MOSFET. The images are taken by AFM at the top of the outermost SnO_2 and SiO_2 layer respectively.

The LbL assembly process for semiconducting and insulating thin films was monitored by the Quartz Crystal Microbalance (QCM, USI-System, Japan) technique. The QCM resonator was immersed in a solution for a given period of time and dried in a nitrogen stream. A decrease of frequency is expected if additional mass is adsorbed onto it. The step growth monitored by QCM is shown in Fig. 5.2 (a). The right vertical axis is the frequency shift, and the left one stands for the thickness converted from the frequency shift. At the first stage, a well-defined precursor film containing four polyion layers in the alternate mode of PDDA /PSS was coated onto resonators. Next, the SnO_2 was adsorbed in alternation with PDDA followed by 6 layers of SiO_2/PDDA. This process was periodically interrupted for the purpose of measuring the QCM resonance frequency. Fig. 5.2 (a) indicates that the growth step of the nanoparticles was much larger than the polyion layers.

The AFM images of LbL self-assembled insulating and semiconducting layers are shown in structural schematic of Fig. 5.1. The images are a top view of those nanoparticle multilayers. One can see multilayers with closely packed nanoparticles and a smooth surface. These results demonstrate an ability to build up vertical nanoscale structures for microelectronic devices with LbL technique. The growth of the nanoparticles was linear and stable with an increment of about 30 nm for one bilayer. The polymer PDDA interlayer thickness was no more than 1-2 nm. The growth step of the SnO_2/PDDA bilayer was 28 nm and the thickness of 6 bilayers was 170 nm including 25 nm precursor polymer layers. The growth step of the SiO_2/PDDA bilayer was 30 nm, and for 6 bilayers this gave 180 nm. The total thickness of the nanoparticle layer was 375 nm as one can conclude from QCM data (Fig 5.2 a). Including the 200-nm top aluminum

layer, the total thickness of the device is 575 nm. This is in good agreement with the device thickness measured by the 2D profilometer, as shown in Fig. 5.2. This plot can serve as the construction map for the device fabrication of the same type of nanoparticles.
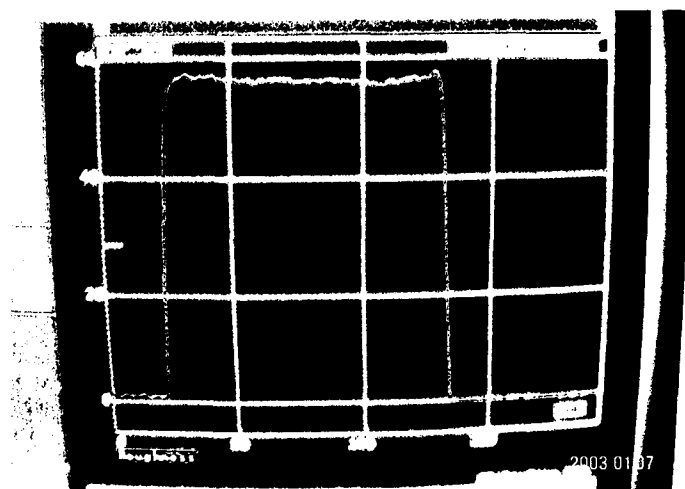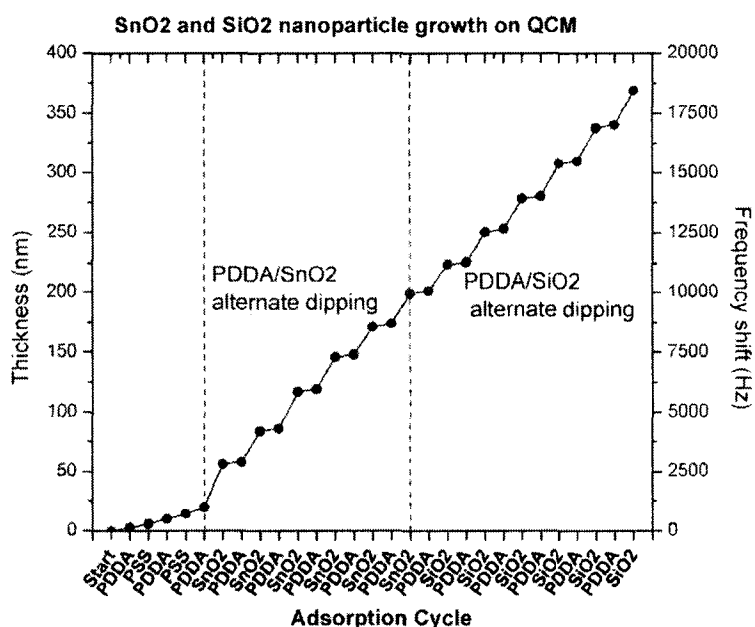
Fig. 5.2 (Top) The adsorption of SnO$_2$ (15 nm) and SiO$_2$ (45 nm) nanoparticles on QCM, the first 5 steps are the precursor layer; then 6 layers of SnO$_2$ and SiO$_2$ are adsorbed in alternate with PDDA. The right vertical axis is the frequency shift and the left one is calculated thickness. (Bottom) The thickness measured by Tencor profilometer, about 575 nm, is in agreement with the one calculated by Sauerbrey equation. The unit of y-axis is 10 nm and x-axis is μm.

<u>Electronic Characteristics</u>

A high reproducibility was achieved in electrical characteristics for forty MOSFET devices fabricated on the same silicon wafer. Many of the MOSFETs were tested and they all gave an identical characterization. The I_{DS}-V_D drain characteristics and gate transfer characteristics of the MOSFET are shown in Fig. 5.3. The MOSFET has a channel length and width of 5 and 100 μm, respectively, and a dielectric thickness of 267 nm. The source and the drain are made of titanium, and the gate is formed by aluminum. The drain current increases with the gate voltages from 0 to 6 V at a step of 545 mV. To analyze the electrical performance of the MOSFET, we assume that the traditional theory is effective (33). Under this circumstance, the conductive channel induced by the gate voltage is an n-channel with electrons as the carrier. By linearly extrapolating the gate transfer curve to the V(G) axis, the threshold voltage Vth can be extracted to be 3 V. In the conventional theory, the drain current in the linear and saturation region can be expressed as:

$$I_{Dlinear} = \frac{W\mu_{FET}C_i}{L}V_D(V_g - V_{th})$$ (2)

$$I_{Dsat} = \frac{W\mu_{FET}C_i}{2L}(V_g - V_{th})^2$$ (3)

where $I_{Dlinear}$ and I_{Dsat} are the drain current in the linear and saturation regions, W and L are the channel width and length, μFET is the carrier mobility, Vth is the threshold voltage, Ci is the gate dielectric capacitance per unit area, $2 \times 10\text{-}4$ F/m^2 in our early report (25). The electron mobility can be extracted to be $2.1 \times 10\text{-}2$ cm^2/ V·s by inputting all the

parameters including I_{Dsat} and VD into equation 3. From Fig. 5.3 (b), the on/off current

ratio is about 104. The subthreshold slope is 1.75 V/decade. SnO_2 is an n-type, wide-

band-gape (Eg = 3.6 eV) semiconductor with a rutile structure. The electrical

conductivity of SnO2 results primarily from the existence of oxygen vacancies, which act

as donors. From Fig. 5.3 (a), one concludes that this MOSFET is working under carrier

accumulation instead of carrier inversion mode. The characteristics of this nanoparticle-

based MOSFET working under carrier accumulation are similar to a polymeric MOSFET.

This is probably due to the positively charged polyion (PDDA) electrostatically bonded

with SnO_2, showing the electrical characteristics similar to the ones of semiconductive

polymers.

Fig. 5.3 (Top) The drain current-voltage characteristics with gate voltages sweeped from 0 to 6 V in 0.545 V step. The channel width and length are 100 and 5 μm. (Bottom) The transfer characteristics with gate voltages sweeped from 0 to 10 V at V_{DS}=4 V.

In$_2$O$_3$ nanoparticles have been used to replace SnO$_2$ as the active material. The

number of silica layers is increased to 8 in order to eliminate the leakage current from

gate to drain. As shown in figure 5.4, the electrical field effect is apparent and the leakage

current is mainly removed, displaying a current-voltage curve family starting from zero
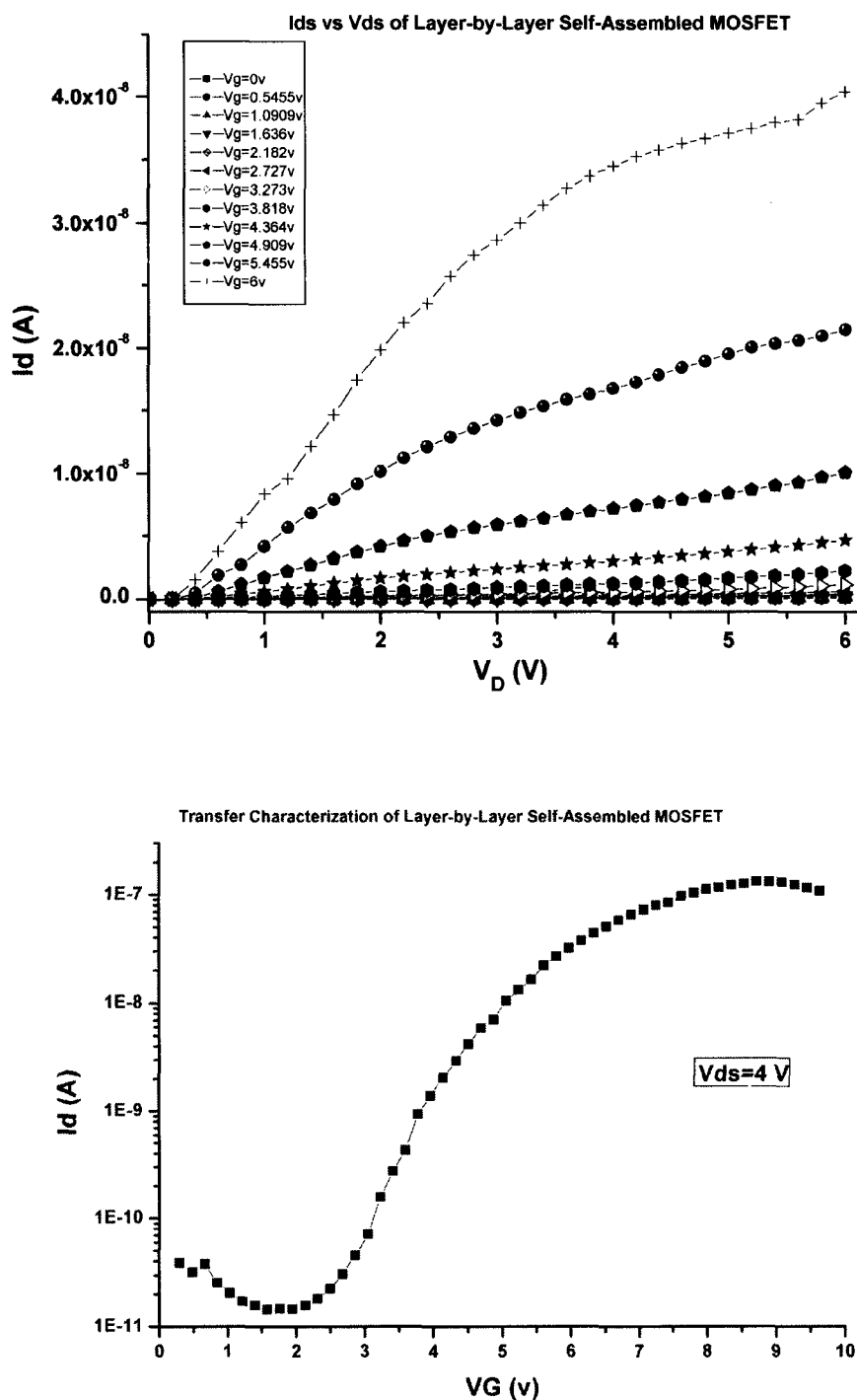
point.
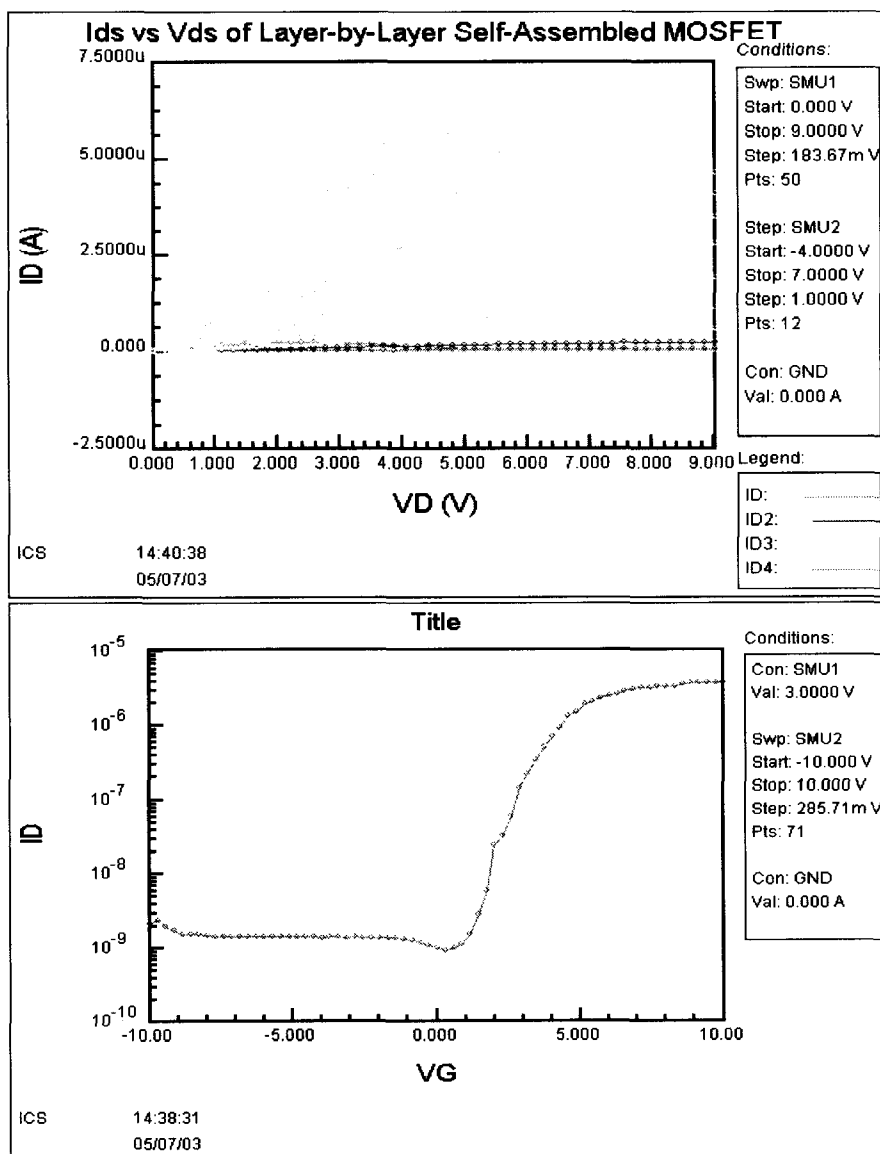
Fig. 5.4 (Top) The drain current-voltage characteristics with gate voltages swept from
0 to 9 V in 0.183 V step. The channel width and length are 100 and 5 μm. (Bottom) The
transfer characteristics with gate voltages swept from -100 to 10 V at V$_{DS}$=3 V.

This proves that the layer-by-layer self-assembled nanoparticle thin film on the silicon wafer can be incorporated into a microelectronic device and function as the conventional one. The thickness of each layer in the device can be under precise control and the composition of the multilayer predesigned by designing the sequence of the deposition. The modified lithography technique fits the patterning of the layer-by-layer self-assembled thin film.

CHAPTER VI

MAGNETIC THIN FILM CANTILEVER

6.1.   Fabrication &Structure

The new layered multilayer with ordered, composite, and functional architecture in nanometer scale has emerged to serve as the basic component of complex devices. Its synthesis on solid surfaces by building blocks such as polyelectrolytes, nanocrystals, and enzymes has been attracting research attention in the fields of optoelectronics, catalysis, and biochemistry. The capability of engineering the material in size and functionality in a wide range allows the compositional and architectural control of the multilayer. By exploiting the currently popular synthetic method, self-assembly, new materials in nanoscale have been created and integrated into devices and systems.

In this chapter, a concept is presented to synthesize a multilayer thin film cantilever. The cantilever consists of body which is detached from the substrate and root which anchors on the substrate. The size of the cantilever in this chapter is 1x2 mm. The cantilever is actually a composite multilayer comprised of Polydiallyldimethylammonium chloride (PDDA), clay and black iron oxide nanocrystal, as shown in figure 6.1. Each monolayer is constructed by the LbL self-assembly which is based on alternate electrostatic adsorption of components (polymers, nanoparticles, or proteins). Materials in each monolayer are adsorbed onto the substrate from aqueous solution by a

75

series of dipping coatings in a predesigned sequence. The oppositely charged materials are coated onto each other by the electrostatic interaction. Almost unlimited number of layers can be deposited one on another by each immersion in the aqueous solution. Each layer exhibits its own function as per the design. By the same reason, the adsorption of layered structure is undergone by only two beakers under room temperature. The growth step is largely determined by the size of the adsorbate. Although the number of layer is large, the distribution of material and monolayer thickness is still absolutely known. In well-established LbL self-assembly, PDDA usually serves as the positively charged polyelectrolyte glue to get the other two layers together. Clay is added into the multilayer to dramatically strengthen the structure. Under the scanning electron microscope, clay has a shape like a laminated flake that covers the entire surface. It tends to grasp the discrete adsorbed substance, making the structure more steadfast. Fe_3O_4 powder is integrated into the cantilever as the magnetic nanocrystal which will eventually make the cantilever magnetic sensitive. Apparently, the size, flexibility and functionality can be adjusted freely in a wide range by changing the number of layers, amount of clay and type of nanocrystal. In this experiment, the magnetic nanocrystal were integrated into the cantilever, creating a structure from which a magnetometer may finally be derived and which will correspond to the external magnetic field. Let's imagine that groups of cantilever be implanted along the fluidic channel and a one-directional magnetic field sweeps at regular frequency, they may function as a micropump. So, the micropump may be replaced and the leaking problem permanently solved. If the magnetic multilayer encapsulates a core, it may realize material delivery by magnetic force. Furthermore, the

concept of multilayer of self-assembled thin films may extend its application to other fields. For example, if the nanocrystal is replaced by TiO_2, it may act as the gas sensor.

Before the multilayer begins to be built, each adsorbate is measured for its surface charge by the zeta potential analyzer. Since the deposition relies on the electrostatic attraction, the knowledge of the surface charge helps determine the polyion that possesses an opposite charge. The zeta potential of clay and Fe_3O_4 are -50 and -40 mv respectively, showing a strong surface electrostatic force. Therefore, positively charged PDDA is selected to coat in alternate with them. In this experiment, the coating sequence is [PDDA (10min) +PSS (10min)]$_2$ +{PDDA (10min) +Fe_3O_4 (15min) + [PDDA (10min) +Clay (8min)]$_2$ +PDDA (10min) +Fe_3O_4 (15min) +PDDA (10min) +Clay (8 min)}$_3$. The first two precursor layers containing PDDA and PSS are coated in order to prepare for a smooth and uniform base for the subsequent coating. The amount of Fe_3O_4 and clay in the next coating is optimized to make the multilayer strong, flexible and sensitive. The thickness of the multilayer is under precise control because each growth step is highly stable. The quartz crystal microbalance (QCM) technique allows us to monitor the growth of thin film by detecting the frequency shift of the QCM. As shown in figure 6.2, in average, one cycle of clay and Fe_3O_4 adsorption gives the thickness increase of 25 nm. The total thickness should be about 400 nm for the adsorption process described above. The real thickness of the multilayer is measured to be 0.45 μm by a surface profiler.

The patterning of the cantilever and detaching of the body is realized by traditional lithography. Figure 6.3 displays the schematic of the cantilever synthesis. Poly (diallyldimethylammonium chloride), MW 200-300K (PDDA, Aldrich), and sodium poly (styrenesulfonate), MW 70,000 (PSS, Aldrich), were used at a concentration of 1.5 -

3 mg/ml. Clay and Fe3O4 powder were diluted in DI water to provide concentrations of 6.5 mg/ml and 4 mg/ml respectively. The suspensions were stirred up completely and ultrasonicated for 30 min. After another 30 min precipitation, the aggregated clusters were removed.

Initially, the 4-inch silicon wafer was put into sulfuric acid and hydrogen peroxide solution (volume ratio 3:7) at 70°C for 1 hour. The wafer was completely rinsed by DI water and baked on a hotplate at 150°C for 3 min. Two layers of positive resist (PR1813) were coated at the maximum speed of 1000 rpm for 40 seconds. The wafer with photoresist was baked on a hotplate at 150°C for 80 seconds. The resist was subsequently exposed by UV light for 20 s. Next, it was immersed in developer solution (MF-319). At this point, the bar was transferred onto the resist. After realigning the mask to the resist, the resist was exposed a second time.

Following the above steps, LbL assembly of clay and Fe_3O_4 was implemented on the silicon wafer. The sequence of the alternate immersion was [PDDA (10min) +PSS (10min)]$_2$ +{PDDA (10min) + Fe_3O_4 (15min) +[PDDA (10min) +Clay (8min)]$_2$ +PDDA (10min) +Fe_3O_4 (15min) +PDDA (10min) +Clay(8 min)}$_3$. Intermediate rinsing and drying after each immersion was necessary. The rinsing was done by purging the wafer in DI water flow for 1 minute. The drying was carried out by nitrogen stream. Subsequently, the wafer was soaked into developer solution to remove the photoresist and multilayer above it, with assistance of ultrasonication for 2 s. The wafer was kept wet and exposed again. It was put in developer until the cantilever is freestanding.

Positive photoresist was coated on the silicon wafer. The first lithography and develop created a bar on the resist. The second UV irradiation exposed the entire resist

area except those which will become the body of cantilever. But this time, the resist was not developed. The exposure of UV light led to an optochemistry reaction in the resist making it soluble in developer while the unexposed area remained insoluble. Then the adsorption process described above began. Between every two adsorption, the rinsing by DI water and drying was necessary to keep the newly grown film clean and stable. After the adsorption, the multilayer thin film sticked to three areas: the silicon surface in the bar, the unexposed and exposed resist surface. The wafer was soaked in developer to dissolve the UV light exposed resist. When this portion of resist was dissolved, the thin film above it would also be peeled off if appropriate external force was introduced such as ultrasonication (very short time). The remained resist was irradiated by UV light for adequate time to make sure it is completely exposed. Eventually, the remaining resist was slowly dissolved in developer solution and the multilayer film above it became freestanding in the solution. The unexposed resist could be dissolved by acetone directly without being exposed again. Yet it was not preferred because the thin film was more stable in MF-319 developer solution.

6.2. Results and Discussion

Figure 6.4(a) displays the cantilever before detached from the silicon wafer. Figure 6.44(b) shows the top view of the freestanding cantilever. Other images of figure 6.4 show various positions of the magnetic film under external magnetic field from above. The film stands up at a different angle in according to the change of the magnetic field. The thin film prepared by this method is steadfast and flexible. The bending angle can be readily reached over 90 degrees and restored immediately if the magnetic field disappears.

Such up-down movement of the cantilever can be repeated for many times without showing any sign of fatigue or damage to the structure. Figure 6.4(h) displays a totally detached film floating in the water which can be operated by tweezers. The explanation may come from the Sem image (figure 6.5) of the thin film surface, showing Fe_3O_4 nanocrystals connected by glue like clay layers.

In summary, we have developed a synthetic technique for a layer-by-layer self-assembled thin film cantilever. The dimension, performance and strength can be adjusted in a wide range. The clay is used to strengthen the structure. It will find applications in sensors and actuators if the appropriate functional substance is integrated in.
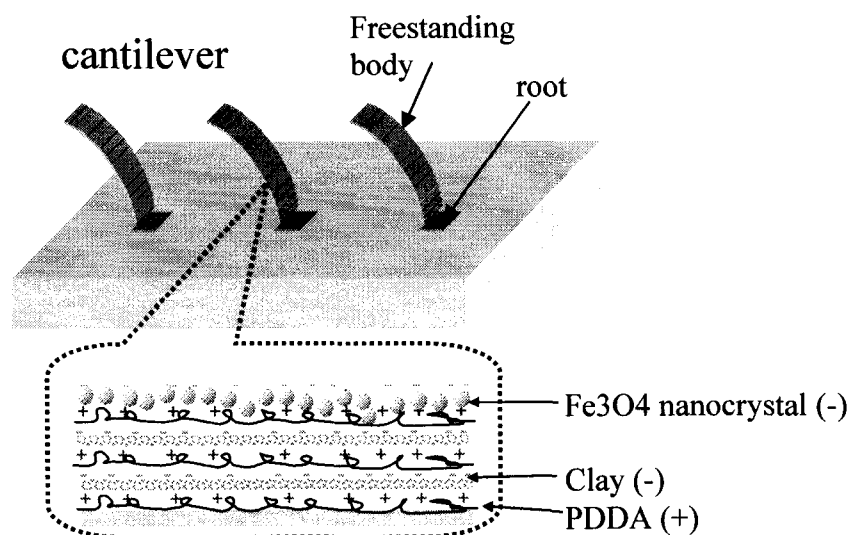

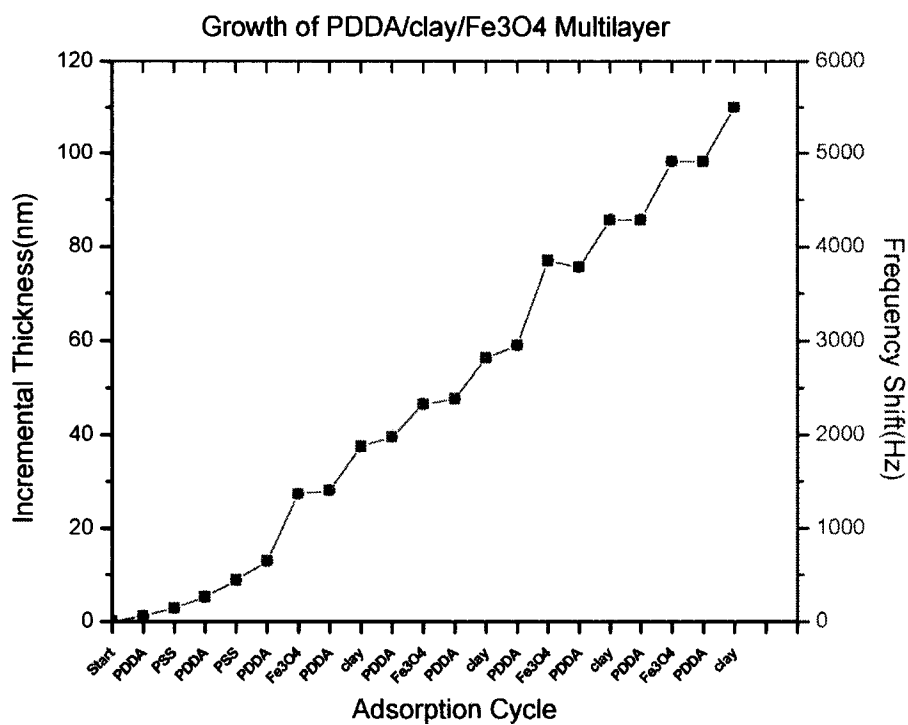Figure 6.1. Schematic of the magnetic thin film cantilever. It is comprised of layers of PDDA/Clay/Fe3O4 nanocrystal

Figure 6.2. The QCM monitoring of multilayer growth in a coating sequence of PDDA/Fe3O4/PDDA/clay. The first 4 layers of PDDA/PSS are the precursor before the coating.

(1) Coat photoresist on silicon wafer

(2) Pattern a bar on the resist

Exposed by UV light, Unexposed, insoluble
soluble

(3) Expose the yellow area by UV light while the red areas are remained unexposed

(4) Layer-by-layer self-assemble multilayer of PDDA/Fe₃O₄/clay

(4) Lift-off by dissolving the exposed resist. Expose the remaining resist.

(5) Dissolve the resist to make the cantilever freestanding.
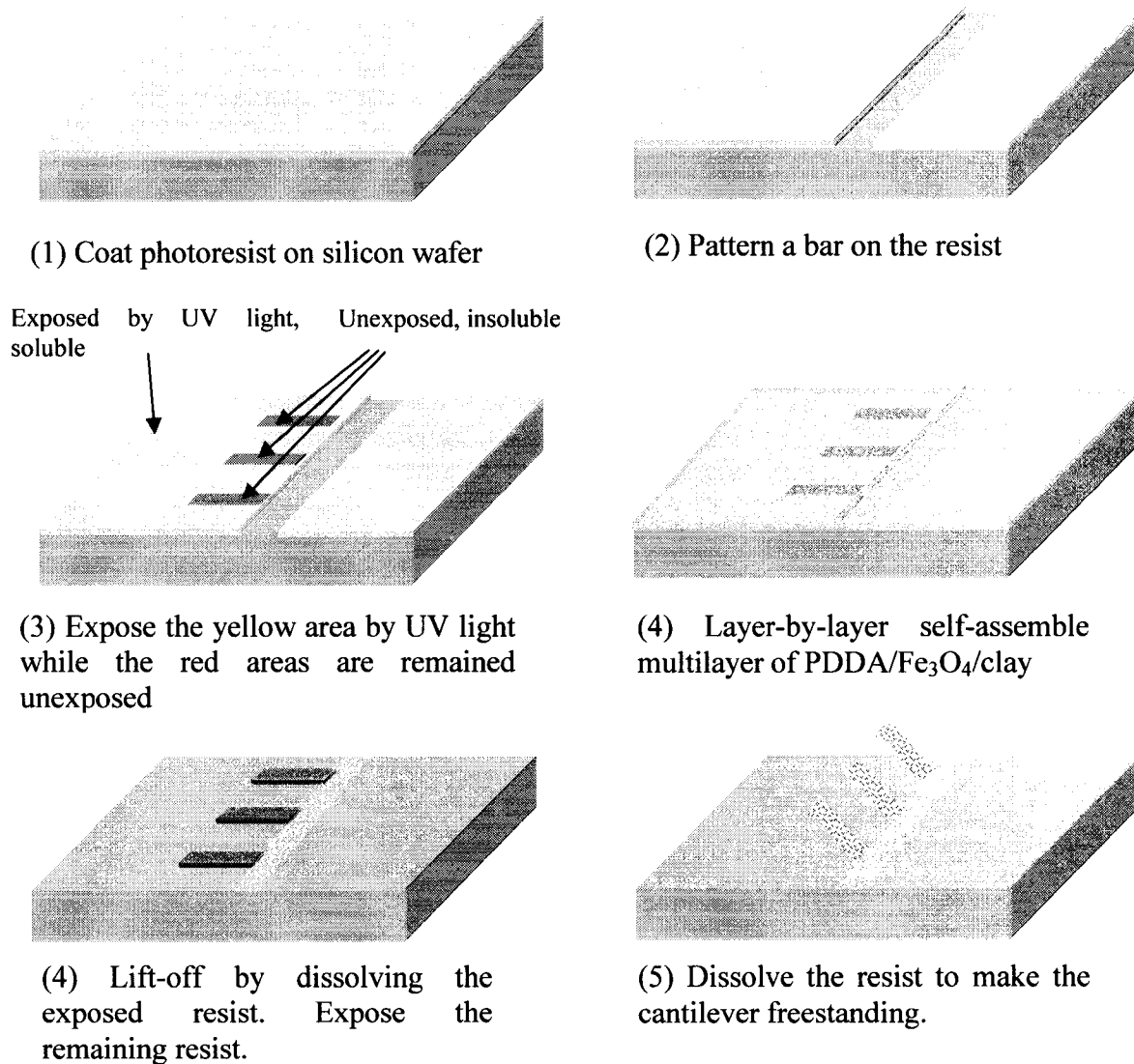
Figure 6.3. Schematic of the fabrication of the thin film cantilever
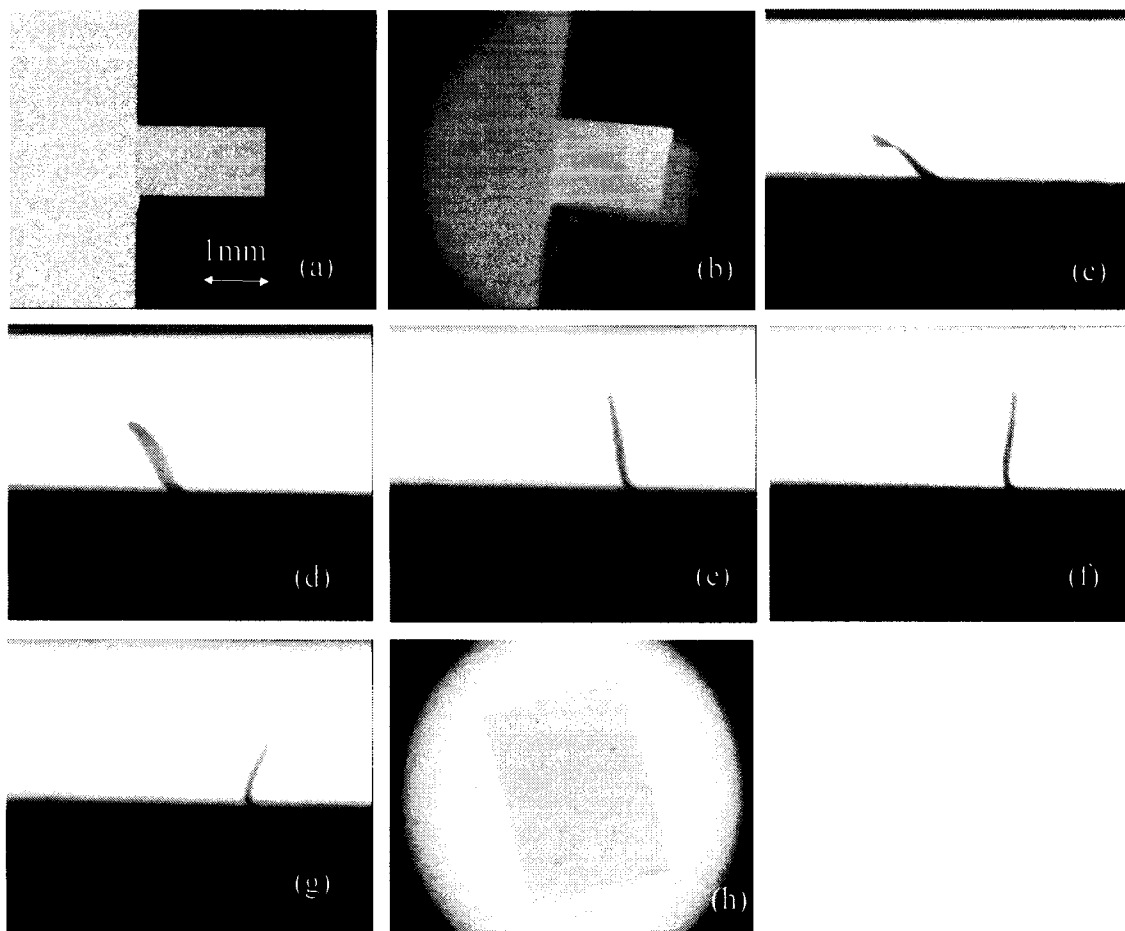
Figure 6.4. (a) The top view of cantilever before being released. (b) Freestanding cantilever (c)-(g) The respond of the magnetic cantilever when the magnetic field changes. (h) A multilayer thin film floating in the water.
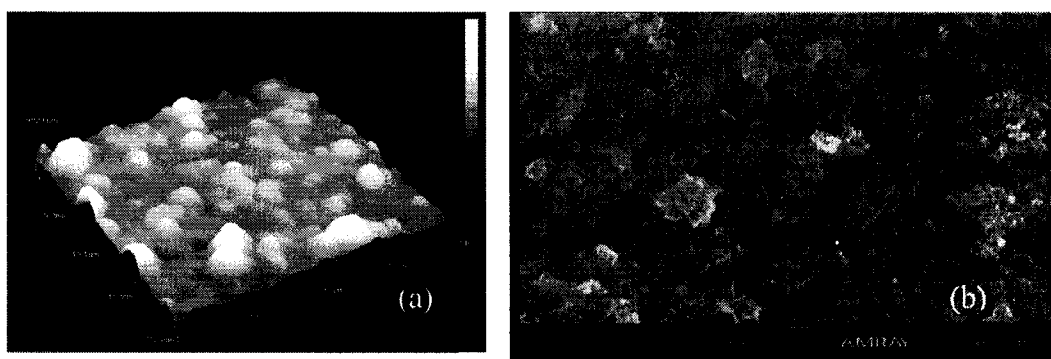

Figure 6.5. (a) Atomic force micrographs of the multilayer surface. (b) SEM image of the multilayer surface.

CHAPTER VII

SUMMARY AND FUTURE WORKS

Novel building blocks such as polyion, nanoparticle and clay nanoplate have been successfully coated on a solid substrate from aqueous solution by LbL self-assembly. Precise control of the size and composite is demonstrated. The newly synthesized multilayer thereby demonstrates robust structure and versatile functionality. The number of layers in the multilayer is almost unlimited. The quality of the such-produced thin film is high enough to perform properly in thin film devices, i. e. the surface is the smooth and a dense structure exists.

The LbL self-assembly technique is assisted by a conventional semiconductive process to construct complex structures on the thin film. The modified process possesses the capability of spatially patterning LbL self-assembled substances on the silicon wafer. This process is stable in micro-scale.

Thin film devices are therefore fabricated by the thin films produced in this way. This technique is classified into the down-top technique which is promising in device fabrication with higher resolution. An MOS-capacitor, MOSFET and a magnetic thin film cantilever have been fabricated. Their performance is satisfactory compared to the conventional ones while the cost and process are significantly reduced and simplified.

This technique can find applications in device and system fabrication based on LbL self-assembled thin films on different substrates including plastic.

However, the patterning technique is still only stable at the micrometer level. With the continuous downscaling of the device, a nanometer scale patterning technique should be developed which is reliable over a large area.

Other devices which have cavity in its structure will be considered to take advantage of LbL self-assembly to coat a uniform layer even on the inner wall of the cavity, which is hard to fulfill by conventional coating methods.

REFERENCES:

1. G. Decher, *Science,* 1997, 21, 227.

2. S. Keller, H. N. Kim, and T. Mallouk, *J.Am. Chem. Soc.* 1994, 116, 8817.

3. Y. Lvov, G. Decher, and H. Mohwald, *Langmuir* 1993, 9, 481.

4. Y. Lvov, G. Decher, and G. Sukhorukov, *Macromolecules,* 1993, 26, 5396.

5. G. Decher, Y. Lvov, J. Schmitt, *Thin Solid Films* 1994, 244, 772.

6. G. Mao, Y. Tsao, M. Tirrell, H. Davis, V. Hessel, and H. Ringsdorf, *Langmuir,* 1993, 9, 3461.

7. D. Korneev, Y. Lvov, G. Decher, J. Schmitt, and S. Yarodaikin, *Physica B* 1995, 214, 954.

8. Lvov, Y.; Ariga, K.; Ichinose, I.; Kunitake, T. *Langmuir* 1997, 13, 6195

9. Takeshi, S.; Satoko K. *Colloids and Surfaces.* 2000, 164, 237

10. D. Yoo, S. Shiratori, S. Rubner, *Macromolecules,* 1998, 31, 4309.

11. Decher. G, E. Michel, J. Schmitt and B. Struth, Colloidal & Interface Sci, 1998, 3, 77

12. Y. Lvov, Chapter 4 Handbook of Surfaces and Interfaces of Materials, Editor: H.S. Nalwa, p. 170-189.

13. J. Cheung, A. Fou, and M. Rubner, *Thin Solid Films* 1994, 244, 985

14. M. Ferreira and M. Rubner, *Macromolecules,* 1995, 28, 7107

15. J. Cheung, W. Stockton, and M. Rubner, *Macromolecules,* 1997, 30, 2712

16. P. Hammond and G. Whitesides, *Macromolecules* 1995, 28, 7569

17. S. Clark, M. Montague, and P. Hammond, *Macromolecules,* 1997, 30, 7237

18. V. Tsukruk, V. Bliznyuk, d. Visser, A. Campbell, T. Bunig, *Macromolecules* 1997, 30, 6615

19. Y. Lvov, K. Ariga, I. Ichinose, and T. Kunitake, *J. Am. Chem. Soc.* 1995, 117, 6117

20. Y. Lvov, K. Ariga, I. Ichinose, and T. Kunitake, *J. Chem. Soc. Chem. Commun.* 1995, 2313

21. M. Sano, Y. Lvov, and T. Kunitake, *Ann. Rev. Mater. Sci.* 1996, 26, 153

22. I. Ichinose, K. Fujiyoshi, S. Mazurka, Y. Lvov, and T. Kunitake, *Chem. Lett,* 1996, 257

23. F. Caruso, K. Niikura, N. Furlong, and Y. Okahata, *Langmuir* 1997, 13, 3427

24. N. Hoogeveen, M. Cohen Stuart, and G. Fleer, *Langmuir,* 1996, 12, 3675

25. Y. Lvov, K. Ariga, and T. Kunitake, *Colloids Surf. A*, 1999, 146, 337

26. R. Ivkov, S. Satija, Y. Lvov, J. Rusling, B. Gaber, and R. Price, *Thin Solid Films*, 2001, 358, 300

27. G. Decher, M. Eckle, J. Schmitt, and B. Struth, Curr. Opin, *Colloid Interf. Sci.* 1998, 3, 32

28. T. Farhat, G. Yassin, S. Dubas, and J. Schlenoff, *Langmuir* 1999, 15, 6621

29. Y. Lvov, M. Onda, K. Ariga, and T. Kunitake, *J. Biomater. Sci. Polym. Ed.* 1998, 9, 345

30. M. Onda, K. Ariga, and T. Kunitake, J. Ferment. *Bioeng.* 1999, 87, 69

31. A. Rogach, A. Susha, F. Caruso, G. Sukhorukov, A. Kornowski, S. Kershaw, H. Mōhwald, A. Eychmüller, and H. Weller, *Adv. Mat.* 2000, 12, 333

32. O. Mitsuyoshi, N. Hiroshi, Y. Takahiro and Y. Katsumi, *Jpn. J. Appl. Phys.* 1997, 36, 5322

33. O. Onitsuka, A. C. Fou, M. Ferreira, B. R. Hsieh and M. F. Rubner, *J. Appl. Phys,* 1996, 413, 395

34. J. Halls, C. Walsh, N. Greenham, E. Marseglia, R. Friend, S. Moratti and A. Holmes, *Nature,* 1995, 376, 498

35. Gang Chen, *Journal of Nanoparticle Research*, 2000, 2, 199–204.

36. Y. Takeda , V.T. Gritsyna , N. Umeda , C.G. Lee , *Nuclear Instruments and Methods in Physics Research B*, 1999, 148, 1029-1033

37. B. O. Dabbousi, J. Rodriguez-Viejo, F. V. Mikulec, J. R. Heine, H. Mattoussi, *J. Phys. Chem. B*, 1997, 101, 9463

38. T. Mimani , K. C. Patil, *Mater.Phys.Mech.*, 2001, 4, 134

39. Chen, K.; Jiang, X.; Kimerling, L.; Hammond, P. *Langmuir* 2000, 16, 7825.

40. Jiang, X.; Hammond, P. *Langmuir* 2000, 16, 8501.

41. Jiang, X.; Zheng, H.; Gourdin, S.; Hammond, P. *Langmuir* 2002, 18, 2607.

42. Zheng, H.; Lee, I.; Rubner, M.; Hammond, P. *Adv. Mat.* 2002, 14, 681.

43. Kim, E.; Xia, Y.; Whitesides, G. *Adv. Mat.* 1996, 8, 245.

44. Vargo, T.; Calvert, J.; Wynne, K.; Avlyanov, J.; MacDiarmid, A.; Rubner, M. *Supramol. Sci.* 1995, 2, 169.

45. M. Torsten, G. Annamaria, J. Phys. D: *Appl. Phys*, 1996, 29, 340

46. C. Haynes, R. Van Duyne, *J. Phys. Chem. B*, 2001, 105, 5599

47. C. Hulteen, A. Treichel, *J. Phys. Chem. B*, 1999, 103, 3854

48. W. L. W. Hau, D. W. Trau, N. J. Sucher, M. Wong and Y. Zohar, *IEEE*. 2002.

49. F. Hua, Y.Lvov, T. Cui, *Journal of Nanoscience and Nanotechnology*. 2002, 2, 357

50. F. Hua, T. Cui, Y. Lvov, *Langmuir*, 2002, 18, 6712

51. F. Hua, J. Shi, Y. Lvov, and T. Cui, *Nano Lett*, 2002, 2, 1219

52. Nina I. Kovtyukhova, Benjamin R. Martin, Jeremiah K. N. Mbindyo, Peter A. Smith, Baharak Razavi, Theresa S. Mayer, and Thomas E. Mallouk, *J. Phys. Chem. B*, 2001, 105, 8762

53. Thierry Cassagneau, Janos H. Fendler, and Thomas E. Mallouk, *Langmuir* 2000, 16, 241

54. Noriko Saito, Hajime Haneda, Takashi Sekiguchi, Naoki Ohashi, Isao Sakaguchi, and Kunihito Koumoto, *Adv. Mater.* 2002. 14, 418

55. F. Hua, J. Shi, Y. Lvov, and T. Cui, "Fabrication and Characterization of MOS-Capacitor Based on Layer-by-Layer Self-Assembled Thin Films", *Nanotechnology*, 2003, 14, 453

56. Baur C.; Bugacov A.; Koel B. E. *Nanotechnology*, 1998,9, 360

57. S. A. Carter, J. C. Scott, P. J. Brock, *Appl. Phys. Lett.* 1997, 71, 1145-1147

58. J. Shi, F. Hua, T. Cui and Y. Lvov, *Chem Lett.* 2003, 32, 316